NTNU
Norwegian University of
Science and Technology

Large Time Step Explicit Schemes for Partial Differential Evolution Equations

Anders Aase Solberg

NTNU
Norwegian University
of Science and Technology

Department of Energy
and Process Engineering

EPT-M-2016-124

MASTER THESIS

for

Student
Anders Aase Solberg

Spring 2016

Large Time Step explicit schemes for partial differential evolution equations

Eksplisitte skjema med høye tidssteg for partielle differensielle evolusjonslikninger

Background and objective

In 1982, Randall LeVeque proposed a Large Time Step extension of the Godunov scheme for hyperbolic conservation laws. During his project thesis in the fall of 2015, Anders Aase Solberg was able to derive a closed form expression for this scheme. Together with previous work performed by SINTEF and NTNU students, this led to a paper entitled "Large Time Step TVD schemes for hyperbolic conservation laws", submitted for publication in the *SIAM Journal on Numerical Analysis*.

In this paper, a general framework for constructing Large Time Step explicit schemes was studied. This forms a foundation for more detailed studies on how to construct concrete schemes with desirable *accuracy, robustness* and *efficiency* properties. Such studies will be performed in this thesis. Some ideas that could be pursued are:

1) Investigate linear stability properties of LTS through von Neumann analysis
2) Use the modified equation analysis to construct explicit LTS schemes for convection-diffusion equations.
3) Construct optimal ways to add numerical diffusion to LTS schemes to increase robustness.

The investigations of the thesis are expected to lead to concrete suggestions for formulations of LTS schemes.

The following tasks are to be considered:

1. Decide on ideas to pursue that will lead to concrete new fundamental insights on LTS. Herein, the suggestions 1), 2) and 3) may serve as inspiration.
2. Pursue the selected ideas to formulate concrete LTS schemes with quantifiable properties in terms of accuracy, robustness and/or efficiency for evolution PDEs.
3. Verify the properties of the schemes through numerical examples.

Within 14 days of receiving the written text on the master thesis, the candidate shall submit a research plan for his project to the department.

When the thesis is evaluated, emphasis is put on processing of the results, and that they are presented in tabular and/or graphic form in a clear manner, and that they are analyzed carefully.

The thesis should be formulated as a research report with summary both in English and Norwegian, conclusion, literature references, table of contents etc. During the preparation of the text, the candidate should make an effort to produce a well-structured and easily readable report. In order to ease the evaluation of the thesis, it is important that the cross-references are correct. In the making of the report, strong emphasis should be placed on both a thorough discussion of the results and an orderly presentation.

The candidate is requested to initiate and keep close contact with his/her academic supervisor(s) throughout the working period. The candidate must follow the rules and regulations of NTNU as well as passive directions given by the Department of Energy and Process Engineering.

Risk assessment of the candidate's work shall be carried out according to the department's procedures. The risk assessment must be documented and included as part of the final report. Events related to the candidate's work adversely affecting the health, safety or security, must be documented and included as part of the final report. If the documentation on risk assessment represents a large number of pages, the full version is to be submitted electronically to the supervisor and an excerpt is included in the report.

Pursuant to "Regulations concerning the supplementary provisions to the technology study program/Master of Science" at NTNU §20, the Department reserves the permission to utilize all the results and data for teaching and research purposes as well as in future publications.

The final report is to be submitted digitally in DAIM. An executive summary of the thesis including title, student's name, supervisor's name, year, department name, and NTNU's logo and name, shall be submitted to the department as a separate pdf file. Based on an agreement with the supervisor, the final report and other material and documents may be given to the supervisor in digital format.

☐ Work to be done in lab (Water power lab, Fluids engineering lab, Thermal engineering lab)
☐ Field work

Department of Energy and Process Engineering, 1. June 2016

Olav Bolland
Department Head

Bernhard Müller
Academic Supervisor

Tore Flåtten
Research Advisor:

Abstract

We consider the large time step (LTS) method for hyperbolic conservation laws, originally proposed by LeVeque in a series of papers over thirty years ago. In particular we have designed a local multi-point LTS scheme, denoted LTS Constant-Diffusion-$\hat{k}$ (LTS CD$\hat{k}$) scheme, which possesses an inherent natural mechanism for adding numerical viscosity. With this scheme we observe non-oscillating solutions, where other LTS schemes tend to create spurious oscillations for high Courant numbers. The scheme is first order accurate and total variation diminishing (TVD). Its robustness is evaluated by performing simulations for the Euler equations. With the LTS CD$\hat{k}$ scheme we successfully simulate one of the test cases presented in [*LeVeque, R. J. (1985). A large time step generalization of Godunovs method for systems of conservation laws. SIAM Journal on Numerical Analysis, 22(6):1051–1073.*], which gave poor results with the LTS Godunov scheme. The oscillations observed by LeVeque for high Courant numbers are smeared with our diffusive LTS CD$\hat{k}$ scheme. For all problems considered in this thesis, the LTS CD$\hat{k}$ scheme yields solutions without oscillations. Our LTS CD$\hat{k}$ scheme hence provides a significant improvement in robustness compared to previously studied LTS schemes, and is a main result of this thesis.

We give a recipe for constructing higher order LTS schemes, and analyze convergence for the LTS schemes up to third order applied to the linear advection equation. A second order LTS CD$\hat{k}$ scheme is tested for the Sod shock tube problem, which gives very accurate results, but with some oscillations around discontinuities. These higher order schemes are not TVD. We have performed a von Neumann stability analysis to evaluate if they are linearly stable.

Finally we extend the LTS method to the linear constant coefficient convection-diffusion equation, which is a parabolic partial differential evolution equation, by matching the physical viscosity with the numerical viscosity in the modified equation for the LTS CD$\hat{k}$ scheme. Also for this equation we propose a method for constructing higher order schemes. A convergence analysis is performed for a second order LTS CD$\hat{k}$ scheme for different ratios of convection to diffusion, verifying the expected second order convergence.

Sammendrag

I denne master-oppgaven ser vi nærmere på large time step (LTS) metoden for hyperbolske konserverings lover, presentert av LeVeque i en rekke publikasjoner for over tretti år siden. Mer spesifikt har vi designet et lokalt fler-punkt LTS skjema, gitt navnet LTS Constant-Diffusion-$\hat{k}$ (LTS CD$\hat{k}$), som har en naturlig mekanisme for å innføre numerisk viskositet. Med dette skjemaet observerer vi ingen oscillasjoner i løsningen, der andre LTS skjemaer tenderer til å oscillere for høye Courant tall. Skjemaet er av første orden og den totale variasjonen er minkende (TVD). Robustheten evalueres ved å gjøre simuleringer på Euler ligningene. Spesielt simulerer vi ett test problem presentert i [*LeVeque, R. J. (1985). A large time step generalization of Godunovs method for systems of conservation laws. SIAM Journal on Numerical Analysis, 22(6):1051–1073.*], som gav dårlige resultater for LTS Godunov skjemaet. Oscillasjoner observert av LeVeque for høye Courant tall blir jevnet ut med vårt diffusive LTS CD$\hat{k}$ skjema. Alle simuleringer i denne oppgaven gir løsninger som er uten oscillasjoner når vi bruker LTS CD$\hat{k}$ skjemaet. LTS CD$\hat{k}$ skjemaet er derfor betydelig mer robust sammenlignet med tidligere studerte LTS skjemaer. Skjemaet er et av hoved resultatene i denne oppgaven.

Vi viser hvordan man kan konstruere LTS skjemaer av høyere orden, videre utfører vi en konvergens-analyse av LTS skjemaer opp til tredje orden på den lineære adveksjons ligningen. Et andre ordens LTS CD$\hat{k}$ skjema er brukt på Sod shock tube problemet, noe som gir gode approksimasjoner, men med noen oscillasjoner rundt diskontinuitetene. Disse høyere ordens skjemaene er ikke TVD, derfor har vi gjennomført en von Neumann analyse for å bestemme om de er lineært stabile.

Vi utvider LTS metoden til konveksjons-diffusjons ligningen med konstante koeffisienter, som er en parabolsk partiell differensial ligning, ved å tilpasse den fysiske viskositeten med den numeriske viskositeten i den modifiserte ligningen for LTS CD$\hat{k}$ skjemaet. Også for denne ligningen presenterer vi en metode for å lage høyere ordens skjemaer. En konvergens-analyse blir utført for et andre ordens LTS CD$\hat{k}$ skjema for forskjellige forhold mellom konveksjon og diffusjon. Som forventet observerer vi andre ordens konvergens.

Preface

This master thesis is a continuation of my project work, which covered the derivation of the closed form formula for the LTS Godunov coefficient for a scalar hyperbolic conservation law, presented in [1]. I have therefore included some parts from the project work in the introduction and in section 2.

I want to thank my supervisors; Tore Flåtten (SINTEF Materials and Chemistry) and professor Bernhard Müller (NTNU) for excellent guidance during my project and master thesis. They have been very enthusiastic, and shown great interest in my work, which have given a lot of motivation.

Contents

List of Figures

List of Tables

Nomenclature

$\bar{k}_m$	Wave numbers	j	Spatial index
β	Parameter	k	Stencil width
χ	Box function	L	Length of domain for 1D problem
Δt	Time step size	N	Finite precision variable
Δx	Grid spacing	n	Time index
ϵ	Error	p	Local order of convergence
γ	Ratio of specific heat	Q	Flux conservative coefficients
$\hat{k}$	Stencil width extension	s	Shock speed
λ	Eigenvalue	T	Operator
$\mathcal{A}$	Flux-difference splitting coefficients	U	Discrete variable
$\mathcal{O}$	Order	u	Continuous variable
ν	Kinematic viscosity	v	Velocity
Ω	One dimensional domain	C	Courant number
ρ	Density	CFL	Courant-Friedrichs-Lewy
σ	Numerical diffusion	FVM	Finite Volume Method
a	Advection speed	LTS	Large Time Step
E	Energy	PDE	Partial Differential Equation
F	Numerical flux	TV	Total variation
f	Flux function	TVD	Total variation diminishing
g	Amplification factor		

1 Introduction

1.1 Large time step method

The Large Time Step (LTS) method is characterized by increasing the time increment Δt beyond the Courant-Friedrichs-Lewy (CFL) limit, for explicit numerical approximations. The method was originally developed for hyperbolic conservation laws. Hyperbolic conservation laws considered here are partial differential equations (PDEs) in the form

$$\frac{\partial u}{\partial t} + \frac{\partial f(u)}{\partial x} = 0, \tag{1}$$

$u \in \mathbb{R}^m, \quad f : \mathbb{R}^m \to \mathbb{R}^m, \quad x \in \mathbb{R}$ and $t \in \mathbb{R}^+$, with initial condition

$$u(x, t = 0) = u_0(x). \tag{2}$$

The unknown u is a vector, while $f(u)$ is a flux function. Such equations describe the evolution of conserved quantities, and have a broad area of application like gas flow [2] and traffic flow [3]. In the nonlinear case, the developing solution can be quite complex, with travelling discontinuities called shocks or contact discontinuities. Finding an analytical solution then becomes unmanageable. This motivates us to the development of numerical solutions of equation (1).

The hyperbolicity of the problem implies that information travels at finite speeds in space, given by the real eigenvalues of the Jacobian matrix $\partial f/\partial u$, denoted $\lambda_i, \quad i \in \{1, 2, ..., m\}$. We use an explicit finite volume method (FVM) to solve equation (1) numerically, and the property of finite propagation of information becomes useful. One of the big challenges, using numerical tools on hyperbolic problems, is to approximate the fluxes across the faces of a control volume, so that the solution converges to the correct physical solution and no oscillations occur. When approximating the flux at a cell face, traditional methods like upwind, Godunov and Lax-Friedrichs use adjacent cell averages. These methods have a fundamental limitation, because the cell faces are not allowed to be affected by cell averages further away. For these methods to be stable, we must restrict Δt to prevent information from other cells to interact at the face. To guarantee this property, information can travel no further than one cell. This implies

$$C = \frac{\Delta t}{\Delta x} \max_{i,j}(|\lambda_i(U_j)|) \leq 1. \tag{3}$$

Where C is the Courant number [4]. Δx is the grid spacing and U_j the average value of u in cell j. Information with the largest speed travels a number of cells equal to the Courant number. The traditional way to overcome the time increment restriction (3) has been to use implicit methods. But as the grid is refined, the matrix equation needed to be solved grows larger and larger. Implicit methods can be unconditionally stable. On the other hand some drawbacks are diffusive solutions and computationally expensive algorithms. When using implicit methods, the updated cell value will depend

on the values in the whole computational domain, in the sense that all the previous cell values are present in the matrix equation, which is solved for each time step. In the Large Time Step method we update the cell value with a restricted number of previous cell values. Here we look at a local $(2k + 1)$-point stencil centered around the updated cell, opposed to a 3-point stencil used by the above schemes. The stability criterion (3) is now extended to,

$$C \leq k \tag{4}$$

assuming linear interactions. We see from (3) that we can increase Δt if the grid spacing is held constant. So the desired goal of the LTS method is obtained. As we increase the Courant number, fewer time steps are performed, but each time step will cost more computational time, because the flux computation becomes more involved. The great advantage of the LTS method over implicit methods is that all cell value updates are decoupled, and as a consequence the algorithm is easy to compute in parallel.

1.2   Previous work

The large time step method was first studied by LeVeque in a series of papers [5, 6, 7]. LeVeque developed the LTS Godunov scheme, a generalisation of the traditional Godunov scheme. The framework for his scheme was based on waves travelling further than one cell without any interactions, before averaging the solution inside each cell. his scheme was able to provide remarkably good results for scalar conservation laws, but struggled with oscillations for systems of conservation laws. The method was taken further by Harten [8], who constructed a scheme which made the solution more smeared as the time step increased, avoiding oscillations. More research on large time step methods for higher dimensions has been done in recent years by, among others, Qian and Lee [9, 10] and Morales-Hernández et al. [11]. They have studied LTS schemes for multidimensional problems with a dimensional splitting technique. Examples are the multidimensional compressible Euler equations and shallow water equations.

In this thesis, we continue the work of Lindqvist et al. [1], who built an algebraic framework for LTS schemes with a one to one correspondence to the flux difference splitting framework. The flux-difference splitting framework originates from LeVeque's wave interpretation, and the coefficients are given explicitly by Bore in [12].

1.3   Outline of thesis

The three goals of this master's thesis have been:

- Numerical analysis of LTS schemes.

- Construction of a robust LTS scheme for hyperbolic conservation laws (1).

- Designing of a LTS scheme for the convection-diffusion equation.

More precisely, this thesis is structured as follows. After an introduction to the finite volume method and basic LTS schemes in section 2, we move on to the numerical analysis of a general $(2k+1)$-point stencil LTS scheme in section 3. Here we perform a von Neumann stability analysis [13] of the linear scalar advection equation, which is a linear version of equation (1). Together with the stability analysis, we close this section with a derivation of the modified equation up to second order for a nonlinear LTS scheme and up to third order for a linear LTS scheme.

Further in section 4, we concentrate on building a framework for constructing new LTS schemes with desired properties like robustness and accuracy. Goal two and three are both present in this section, because they are highly connected, as will be clear from the text.

In section 5 we test the numerical performance of the presented LTS schemes. Among the test problems, when considering hyperbolic PDEs, are the inviscid Burgers' equation and the Euler equations. For parabolic PDEs, we test the LTS schemes on the linear convection-diffusion equation. Convergence analysis and comparison with established LTS schemes are performed. At the end in section 6, we conclude on the work and propose further work based on this thesis.

2 Large time step schemes

In this chapter we discuss some important concepts related to the discretization of partial differential evolution equations. We will only focus on fully explicit finite volume schemes.

2.1 The finite volume method

Considering a control volume Ω, the change of the conserved quantity u inside the control volume must equal the net flux of u crossing the boundary $\partial\Omega$. For an arbitrary control volume in 3D we have

$$\frac{\mathrm{d}}{\mathrm{d}t}\int_\Omega u\mathrm{d}V + \int_{\partial\Omega} f(u)\cdot\hat{n}\mathrm{d}A = 0, \tag{5}$$

where $\hat{n}$ is the outward pointing unit normal on $\partial\Omega$. We derive the finite volume method for a one dimensional domain $\Omega = [x_{\text{left}}, x_{\text{right}}]$

$$\frac{\mathrm{d}}{\mathrm{d}t}\int_\Omega u(x,t)\mathrm{d}x + f(u(x_{\text{right}},t)) - f(u(x_{\text{left}},t)) = 0. \tag{6}$$

Integrating (6) from t_n to $t_{n+1} = t_n + \Delta t$ gives

$$\int_{t_n}^{t_n+\Delta t}\frac{\mathrm{d}}{\mathrm{d}t}\int_\Omega u(x,t)\mathrm{d}x\mathrm{d}t + \int_{t_n}^{t_n+\Delta t} f(u(x_{\text{right}},t)) - f(u(x_{\text{left}},t))\mathrm{d}t = 0. \tag{7}$$

Next we define the average value of u in the domain at time t

$$U(t) \equiv \frac{1}{L}\int_\Omega u(x,t)\mathrm{d}x. \tag{8}$$

$L = x_{\text{right}} - x_{\text{left}}$ is the length of the domain. The fundamental theorem of calculus yields

$$\int_{t_n}^{t_n+\Delta t}\frac{\mathrm{d}}{\mathrm{d}t}LU(t)\mathrm{d}t = L(U(t_{n+1}) - U(t_n)). \tag{9}$$

Finally we define the average flux over the left and right boundaries during Δt

$$F_{\text{left}} \equiv \frac{1}{\Delta t}\int_{t_n}^{t_n+\Delta t} f(u(x_{\text{left}},t))\mathrm{d}t \tag{10}$$

$$F_{\text{right}} \equiv \frac{1}{\Delta t}\int_{t_n}^{t_n+\Delta t} f(u(x_{\text{right}},t))\mathrm{d}t \tag{11}$$

Equation (7) can now be written as

$$U^{n+1} = U^n - \frac{\Delta t}{L}(F_{\text{right}} - F_{\text{left}}), \tag{12}$$

4

where the superscript n represents t_n. Let Ω be divided into j subdomains denoted $\Omega_j \subseteq \Omega$, which represent the spatial discretization. x_j is the point in the middle of each domain, $x_{j-1/2}$ and $x_{j+1/2}$ are the points at the endpoints of each domain. Since (5) holds for any domain, we use it for each subdomain Ω_j and (12) becomes

$$U_j^{n+1} = U_j^n - \frac{\Delta t}{\Delta x}(F_{j+1/2} - F_{j-1/2}) \quad \forall j, \tag{13}$$

where $\Delta x = x_{j+1/2} - x_{j-1/2}$ and $F_{j\pm1/2}$ are the numerical fluxes at $x_{j\pm1/2}$. For a standard 3-point scheme, the average flux $F_{j\pm1/2}$ depends on the adjacent cell averages U_j and $U_{j\pm1}$. Their dependence on U_j and $U_{j\pm1}$ is what differs in these numerical schemes. We write the numerical fluxes as

$$F_{j+1/2} = \frac{1}{2}(f(U_{j+1}) + f(U_j)) - \frac{\Delta x}{2\Delta t}Q_{j+1/2}^0(U_{j+1} - U_j), \tag{14}$$

determined by a dimensionless parameter $Q_{j+1/2}^0$. Equation (13) is in a conservative form, and the fluxes (14) are written in a consistent manner. In the way that $F_{j+1/2}(U_j = u, U_{j+1} = u) = f(u)$ for all values of $Q_{j+1/2}^0$. The flux conservative form can be rewritten into something called flux-difference splitting form, which is nonconservative

$$U_j^{n+1} = U_j^n - (\mathcal{A}_{j-1/2}^{0+}\Delta U_{j-1/2} + \mathcal{A}_{j+1/2}^{0-}\Delta U_{j+1/2}), \tag{15}$$

$$\Delta U_{j+1/2} = U_{j+1} - U_j. \tag{16}$$

Here $\mathcal{A}_{j\mp1/2}^{\pm0}$ are coefficients for how much $\Delta U_{j\mp1/2}$ influences the updated cell average. We will use both formulations in the further analysis.

The averaging operator (8) on the function $u(x, t_n)$ transform $u(x, t_n)$ to a discrete step function

$$U(x, t_n) = \sum_{j=1}^{j_{\max}} U_j^n \chi_{\Omega_j}(x) \tag{17}$$

where

$$\chi_{\Omega_j}(x) = \begin{cases} 1 & \text{if } x \in \Omega_j \\ 0 & \text{if } x \notin \Omega_j \end{cases} \tag{18}$$

Here $j_{\max}$ is the number of partitions of Ω.

2.2 The Riemann problem

The 1D Riemann problem can be stated mathematically as

$$\frac{\partial u}{\partial t} + \frac{\partial f(u)}{\partial x} = 0 \tag{19}$$

with initial condition

$$u(x, t = 0) = \begin{cases} u_L & x < 0 \\ u_R & x > 0 \end{cases} \tag{20}$$

The initial condition consists of piecewise constant values with one single discontinuity at $x = 0$. This problem can be solved exactly in the scalar case, and a simple closed form expression is given by Osher [14]

$$u(x, t) = u(x/t) = u(\zeta) = \begin{cases} \dfrac{\mathrm{d}}{\mathrm{d}\zeta} \left(\max_{v \in [u_L, u_R]} [\zeta v - f(v)] \right) & u_L < u_R \\ \dfrac{\mathrm{d}}{\mathrm{d}\zeta} \left(\min_{v \in [u_R, u_L]} [\zeta v - f(v)] \right) & u_L > u_R \end{cases} \tag{21}$$

The step function (17) can be thought of as a series of independent Riemann problems, where the discontinuities are located at the cell faces. We can now solve the individual Riemann problems, either exactly or approximately, and use the results to obtain a value for u at the cell faces. Finding the numerical fluxes from the exact solution of the Riemann problems is called the Godunov method. The Roe and the Lax-Friedrichs methods are examples for approximate Riemann solvers. As long as $C \leq \frac{1}{2}$, there are no interactions between the Riemann problems. When the Courant number increases, there is a possibility that the evolution of one discontinuity may influence the evolution of a neighbouring discontinuity. In this thesis we simplify such interactions by treating each discontinuity separately and superpose the result.

2.3   First order large time step schemes

A $(2k + 1)$-point stencil is the basis for our LTS schemes. A direct extension of (14) and (15) gives a general large time step scheme, in both the conservative form and the flux-difference splitting formulation;

- Numerical flux in conservative form

$$\begin{aligned} F_{j+1/2} = {}& \frac{1}{2}(f(U_{j+1}) + f(U_j)) - \frac{\Delta x}{2\Delta t} Q^0_{j+1/2}(U_{j+1} - U_j) \\ & - \frac{\Delta x}{\Delta t} \sum_{i=1}^{k-1} (Q^{i-}_{j+1/2-i}\Delta U_{j+1/2-i} + Q^{i+}_{j+1/2+i}\Delta U_{j+1/2+i}). \end{aligned} \tag{22}$$

- Flux-difference splitting formulation

$$U_j^{n+1} = U_j^n - \sum_{i=0}^{k-1} (\mathcal{A}^{i+}_{j-1/2-i}\Delta U_{j-1/2-i} + \mathcal{A}^{i-}_{j+1/2+i}\Delta U_{j+1/2+i}), \tag{23}$$

where $Q^{i\pm}_{j+1/2\mp i}$ and $\mathcal{A}^{i\pm}_{j+1/2\mp i}$ are the flux conservative coefficients and the flux-difference splitting coefficients respectively. The indices specify the position of a discontinuity relative to cell j. Due to the first order approximation of the time derivative, the scheme is only first order accurate in time, except for some special cases where the choice of the $\mathcal{A}$'s or Q's cancel the $\mathcal{O}(\Delta t)$ term and the scheme is second order accurate. We will in this thesis consider a class of schemes which is total variation diminishing (TVD) when applied to scalar conservation laws. This is also a property of the original problem in integral form. Total variation is defined by

$$TV(u(t)) = \int_\Omega \left| \frac{\partial u}{\partial x} \right| \mathrm{d}x \tag{24}$$

in the continuous case and

$$TV(U^n) = \sum_j |U^n_{j+1} - U^n_j| \tag{25}$$

in the discrete case. The total variation must decrease or rather not increase

$$TV(U^{n+1}) \le TV(U^n) \tag{26}$$

in order for the schemes to be TVD. Inserting (23) into (25) gives, by the application of the triangle inequality, the generalization of Harten's theorem [12]. The result gives restrictions on the coefficients in the form of inequalities

$$\mathcal{A}^{(k-1)+}_{j+1/2} \ge 0 \tag{27}$$

$$\mathcal{A}^{i+}_{j+1/2} \ge \mathcal{A}^{(i+1)+}_{j+1/2} \tag{28}$$

$$1 - \mathcal{A}^{0+}_{j+1/2} + \mathcal{A}^{0-}_{j+1/2} \ge 0 \tag{29}$$

$$\mathcal{A}^{(i+1)-}_{j+1/2} \ge \mathcal{A}^{i-}_{j+1/2} \tag{30}$$

$$0 \ge \mathcal{A}^{(k-1)-}_{j+1/2} \tag{31}$$

The coefficients $\mathcal{A}^{i\pm}_{j\mp 1/2\mp i} = \mathcal{A}^{i\pm}(C_{j\mp 1/2\mp i})$ are functions of the local Courant number C

$$C_{j+1/2} = \begin{cases} \frac{\Delta t}{\Delta x} \cdot \frac{f(U_{j+1}) - f(U_j)}{U_{j+1} - U_j} & \text{if } \Delta U_{j+1/2} \ne 0 \\ \frac{\Delta t}{\Delta x} f'(U_j) & \text{if } \Delta U_{j+1/2} = 0 \end{cases} \tag{32}$$

The local Courant number at face $j + 1/2$ is the translated distance of the local discontinuity measured in number of cells. The discontinuity travels with speed s called the shock speed.

$$C = \frac{\Delta t}{\Delta x} s \tag{33}$$

$$s = \begin{cases} \frac{f(U_{j+1}) - f(U_j)}{U_{j+1} - U_j} & \text{if } \Delta U_{j+1/2} \neq 0 \\ f'(U_j) & \text{if } \Delta U_{j+1/2} = 0 \end{cases} \tag{34}$$

This coincides with the exact solution of the Riemann problem, if the physical solution is a shock. Shock formation will depend on the initial values of the Riemann problem and the nature of the flux function $f(u)$.

2.3.1 The LTS Roe scheme

The first scheme presented treats all the Riemann problems as travelling shocks, even when this is not the nature of the solution. The scheme is denoted as the LTS Roe scheme, and the coefficients are explicitly given as

$$\mathcal{A}^{i+}_{j-1/2-i}(C_{j-1/2-i}) = \max(0, \min(C_{j-1/2-i} - i, 1)) \tag{35}$$

$$\mathcal{A}^{i-}_{j+1/2+i}(C_{j+1/2+i}) = \min(0, \max(C_{j+1/2+i} + i, -1)) \tag{36}$$

The scheme is sharp, in the way that it gives a good approximation of evolving shock waves, but it is prone to entropy violations for rarefaction waves. Entropy violations are generated when the Lax entropy condition, i.e, $f'(U_L) > s > f'(U_R)$, is violated. Thus the solution will not converge to the correct physical solution. Some of the problems can be avoided using an entropy fix [15]. Another approach is to change the Courant number by a random amount, so that the Riemann problem never lingers at a cell face. This method was proposed by Lindqvist [16].

2.3.2 The LTS Lax-Friedrichs scheme

Another scheme is the LTS Lax-Friedrichs scheme [12], which defines

$$\mathcal{A}^{i\pm}_{j\mp1/2\mp i}(C_{j\mp1/2\mp i}) = \frac{1}{2k}(C_{j\mp1/2\mp i} \pm k). \tag{37}$$

The coefficients in the LTS Roe scheme vary with i, because it tries to mimic the exact solution. The LTS Lax-Friedrichs scheme on the other hand gives a very rough distribution, so that basically all cells are affected by the propagating Riemann problem. Coefficients on the left side $\mathcal{A}^{i-}$ have equal value and the same applies for the right side $\mathcal{A}^{i+}$. The values on the left and on the right side are weighted according to the value of C. The scheme causes the solution to get smeared over a larger interval.

Both the LTS Roe and the LTS Lax-Friedrichs schemes are TVD. They also represent the boundaries of the entire spectrum of TVD LTS schemes [1]. The LTS Roe scheme is the least diffusive scheme, and the LTS Lax-Friedrichs scheme the most diffusive one.

2.3.3 The LTS Godunov scheme

The coefficients for the LTS Godunov scheme are obtained by tracking the exact solution of each Riemann problem, but in general there is no explicit formula. The closed form expression for the LTS Godunov coefficients in the scalar case is presented in [1, 17]. It is also shown that the LTS Godunov scheme is more or equally diffusive than the LTS Roe scheme and lesser diffusive than the LTS Lax-Friedrichs scheme. The coefficients are given by

$$
U_j^{n+1} = \sum_{i=-(k-1)}^{k-1} \left(\frac{\Delta t}{\Delta x} \mathcal{M}_{j+1/2-i} \left(f(u) - (i-1)\frac{\Delta x}{\Delta t}u \right) \right.
$$
$$
\left. - \frac{\Delta t}{\Delta x} \mathcal{M}_{j+1/2-i} \left(f(u) - i\frac{\Delta x}{\Delta t}u \right) - U_i^n \right), \tag{38}
$$

where

$$
\mathcal{M}_{j+1/2-i}(w(u)) = \begin{cases} \min\limits_{u \in [U_j, U_{j+1}]} w(u) & \text{if } U_j < U_{j+1} \\ \min\limits_{u \in [U_j, U_{j+1}]} w(u) & \text{if } U_j \geq U_{j+1} \end{cases} \tag{39}
$$

3 Numerical analysis of LTS methods

3.1 Von Neumann stability analysis

When we use numerical tools to solve a PDE, we want a solution where the error does not grow unbounded in finite time. The stability analysis determines the behaviour of the solution, and how the error grows. There are many different stability criteria, but we start with the traditional von Neumann analysis, which applies to linear equations with constant coefficients and periodic boundary conditions. In the von Neumann analysis we look at how the error, due to finite arithmetic precision in computers, affects the solution. The error ϵ_j is defined as

$$\epsilon_j = N_j - U_j, \tag{40}$$

where N_j is the finite precision solution to the discretized equation, and U_j the exact. The error is also a solution to the discretized equation [13], and we therefore evolve this error distribution to see how it develops in time. Since the discrete equations for U_j and ϵ_j are the same, the stability analysis can equivalently be performed for U_j instead of ϵ_j.

3.1.1 5-point scheme

We start our von Neumann stability analysis for a general 5-point stencil LTS scheme given in the flux conservative framework.

$$
\begin{aligned}
F_{j+1/2} = \frac{1}{2}(f_j + f_{j+1}) &- \frac{1}{2}Q^0\frac{\Delta x}{\Delta t}(\epsilon_{j+1} - \epsilon_j) \\
&- Q^{1-}\frac{\Delta x}{\Delta t}(\epsilon_j - \epsilon_{j-1}) \\
&- Q^{1+}\frac{\Delta x}{\Delta t}(\epsilon_{j+2} - \epsilon_{j+1})
\end{aligned}
\tag{41}
$$

Since the stability analysis only covers linear equations, a linear flux function is considered $f_j = a\epsilon_j$, where a is the constant advection velocity. The local Courant number is given by

$$C = \frac{\Delta x}{\Delta t}f'(u) = \frac{\Delta x}{\Delta t}a \tag{42}$$

The updated cell value is given by

$$\epsilon_j^{n+1} = \epsilon_j^n - \frac{\Delta t}{\Delta x}(F_{j+1/2}^n - F_{j-1/2}^n) \tag{43}$$

We insert equation (41) into (43) and get

$$
\begin{aligned}
\epsilon_j^{n+1} = \epsilon_j^n &- \frac{a\Delta t}{2\Delta x}(\epsilon_{j+1}^n - \epsilon_{j-1}^n) \\
&+ \frac{1}{2}Q^0(\epsilon_{j+1}^n - 2\epsilon_j^n + \epsilon_{j-1}^n) \\
&+ Q^{1-}(\epsilon_j^n - 2\epsilon_{j-1}^n + \epsilon_{j-2}^n) \\
&+ Q^{1+}(\epsilon_{j+2}^n - 2\epsilon_{j+1}^n + \epsilon_j^n)
\end{aligned}
\tag{44}
$$

The error function $\epsilon_j(x_j, t)$ can be expressed as a finite Fourier series determined by the number of nodal points in the computational length L, with wave numbers $\bar{k}_m = 2\pi m$, $m \in \{0, 1, 2, ..., M-1\}$, $M = L/\Delta x$, assuming periodic boundary conditions

$$
\epsilon_j(x_j, t) = \sum_{m=0}^{M-1} \hat{\epsilon}_m(t)e^{i\bar{k}_m x_j}.
\tag{45}
$$

Inserting the error function ϵ_j into the discrete scheme (44) and using that the vectors $[e^{i\bar{k}_m x_0}, ..., e^{i\bar{k}_m x_{M-1}}]^T$, $\bar{k}_m \in \{0, 2\pi, ..., 2\pi(M-1)\}$ are linearly independent, we get the Fourier coefficient $\hat{\epsilon}_m$ at the next time level

$$
\hat{\epsilon}_m^{n+1} = g(\bar{k}_m \Delta x)\hat{\epsilon}_m^n.
\tag{46}
$$

Here $g(\bar{k}_m \Delta x)$ is the amplification factor, a measure of how much the amplitude of the mth Fourier mode of the error is amplified from time t_n to t_{n+1}. The von Neumann condition requires that the amplification factor satisfy $|g(\bar{k}_m \Delta x)| \leq 1$ for all values of $\bar{k}_m \Delta x$. It is therefore enough to consider only one Fourier mode in the analysis.

We find the amplification factor for the 5-point scheme by replacing the following

- $\epsilon_j^n = \hat{\epsilon}_m^n e^{i\bar{k}_m x_j}$

- $\epsilon_j^{n+1} = \hat{\epsilon}_m^{n+1} e^{i\bar{k}_m x_j}$

- $\epsilon_{j+l}^n = \hat{\epsilon}_m^n e^{i\bar{k}_m x_{j+l}}, \quad l \in \{-2, -1, 1, 2\}$

Equation (44) then becomes upon dividing by $\hat{\epsilon}_m^n e^{i\bar{k}_m x_j}$

$$
\begin{aligned}
g(\bar{k}_m \Delta x) = 1 &- \frac{C}{2}(e^{i\bar{k}_m \Delta x} - e^{-i\bar{k}_m \Delta x}) \\
&+ \frac{1}{2}Q^0(e^{i\bar{k}_m \Delta x} - 2 + e^{-i\bar{k}_m \Delta x}) \\
&+ Q^{1-}(1 - 2e^{-i\bar{k}_m \Delta x} + e^{-2i\bar{k}_m \Delta x}) \\
&+ Q^{1+}(e^{2i\bar{k}_m \Delta x} - 2e^{i\bar{k}_m \Delta x} + 1).
\end{aligned}
\tag{47}
$$

11

The amplification factor is generally a complex number, so we take the modulus of equation (47) squared. We introduce the real variable $z = \cos(\bar{k}_m \Delta x)$, which is bounded by $z = -1$ and $z = 1$, and get

$$
\begin{aligned}
|g(z)|^2 = 1 - (1 - z)(2Q^0 + 4z(Q^{1-} + Q^{1+}) \\
+ (z - 1)(Q^0 + 2z(Q^{1-} + Q^{1+}))^2 \\
- (z + 1)(C + 2(z - 1)(Q^{1-} - Q^{1+}))^2).
\end{aligned}
\tag{48}
$$

Given a set of coefficients Q^0, Q^{1-} and Q^{1+}, linear stability for a 5-point stencil is achieved if the inequality $|g(z)|^2 \leq 1$ is satisfied for all allowable values of z. Let $Q^{1-}, Q^{1+} = 0$ and $|C| \leq 1$, then the expression reduces to the standard 3-point stencil. We can easily verify that the limits for linear stability in this case are bounded by the Lax-Wendroff and the Lax-Friedrichs fluxes, with $Q^0 = C^2$ and $Q^0 = 1$ respectively. For the 5-point stencil such analytical boundaries for the linear stability region are not that straightforward to obtain, as we will show next. As a first step, we simplify the above expression with the constraint $Q^{1+} = 0$, assuming $a \geq 0$

$$
\begin{aligned}
|g(z)|^2 = 1 - (1 - z)((1 - z)(Q^0 - 2Q^{1-})(1 - (Q^0 - 2Q^{1-})) \\
+ (z + 1)(Q^0 + 2Q^{1-} - C^2 + 4Q^{1-}(1 - z)(C - Q^0))).
\end{aligned}
\tag{49}
$$

The expression can be rearranged as a polynomial function of $w = 1 - z, w \in [0, 2]$.

$$
|g(z)|^2 = 1 - wA(w)
\tag{50}
$$

where

$$
A(w) = a_2 w^2 + a_1 w + a_0
\tag{51}
$$

is a quadratic polynomial and the coefficients are given by

1. $a_2 = 4Q^{1-}(Q^0 - C)$

2. $a_1 = C^2 - (Q^0 + 2Q^{1-})^2 + 4Q^{1-}(2C - 1)$

3. $a_0 = 2(Q^0 + 2Q^{1-} - C^2) = 2\sigma$

For stability the function $A(w)$ must be positive in its domain. Immediately we see that a necessary condition for linear stability is positive or zero diffusion coefficient, $\sigma \geq 0$. From the modified equation for a general (2k+1)-point scheme we define the diffusion coefficient to be $\sigma = Q^0 + 2\sum_i(Q^{i-} + Q^{i+}) - C^2$ [1], the modified equation is discussed further in section 3.2. Suppose the diffusion coefficient were negative, then an arbitrary value w^+ close to the right of $w = 0$ would, by continuity, lead to a negative value of $A(w^+)$, and hence an unstable scheme. Stability only occurs for negative diffusion when $w = 0$, but this is only a special case and does not cover all

the possible wave numbers. We find other conditions using properties of a quadratic function. First we consider the Courant number in the interval $0 \leq C \leq 1$, and divide into four sub cases.

1. $Q^0 < C$ and $Q^{1-} > 0$

   In this case a_2 is negative and $A(w)$ becomes a concave function. If $A(0) \geq 0$ and $A(2) \geq 0$, we can guarantee that $A(w) \geq 0$ for $w \in [0,2]$. This follows from a property for concave functions. $A(0) \geq 0 \iff \sigma \geq 0$ and $A(2) \geq 0 \iff 0 \leq Q^0 - 2Q^{1-} \leq 1$ together with $Q^0 < C$ and $Q^{1-} > 0$ defines the region of linear stability in this case. $A(0) \geq 0$ and $A(2) \geq 0$ are necessary conditions and are assumed in all the other cases as a lower bound.

2. $Q^0 < C$ and $Q^{1-} < 0$

   The sign of a_2 switches to positive, and the only possible unstable configuration is when the extrema of $A(w)$ are located in the domain. We show that this is not the case. The extreme point is located at $w = -\frac{a_1}{2a_2}$. w is outside the domain if we can prove that $a_1 > 0$.

$$
\begin{aligned}
a_1 &= C^2 - (Q^0)^2 - 4Q^0 Q^{1-} - 4(Q^{1-})^2 + 8Q^{1-}C - 4Q^{1-} \\
&= (C^2 - (Q^0)^2) - 4Q^{1-}(Q^0 + Q^{1-} - 2C + 1).
\end{aligned} \tag{52}
$$

   From $A(0) \geq 0$, we use that $Q^0 \geq C^2 - 2Q^{1-}$. This gives

$$
\begin{aligned}
a_1 &\geq (C^2 - (Q^0)^2) - 4Q^{1-}(C^2 - Q^{1-} - 2C + 1) \\
&= (C^2 - (Q^0)^2) - 4Q^{1-}((C-1)^2 - Q^{1-}). \\
&\geq 0
\end{aligned} \tag{53}
$$

3. $Q^0 > C$ and $Q^{1-} < 0$

   Again a_2 is negative and the only requirements are $A(0) \geq 0$ and $A(2) \geq 0$.

4. $Q^0 > C$ and $Q^{1-} > 0$

   Here a_2 is positive and $A(w)$ becomes a convex function. The position of the global extrema can in this case lie in the interval $[0,2]$, because (53) no longer holds. Therefore we look at two cases. Either the global minimum is positive or negative.

   (a) $a_0 - \frac{a_1^2}{4a_2} > 0$

      This condition gives a linearly stable configuration together with the convex property.

   (b) $a_0 - \frac{a_1^2}{4a_2} < 0$

      We need an extra restriction in addition so that the minimum should not lie in the interval [0,2]: $-\frac{a_1}{2a_2} \notin [0,2]$.

All the cases sum up to the region of linear stability when $0 \leq C \leq 1$. Exploring further with a Courant number in the interval $1 \leq C \leq 2$ eliminates the cases when Q^{1-} is negative and only cases 1 and 4 are present. In figure 1 and 2 we show the linear stability maps composed of the various cases for Courant numbers 0.5 and 1.5. If the coefficients (Q^{1-}, Q^0) are not in the dark blue region in figures 1 and 2, the 5-point stencil LTS scheme (13) with the flux function (41) is stable for the linear advection equation with $a > 0$.
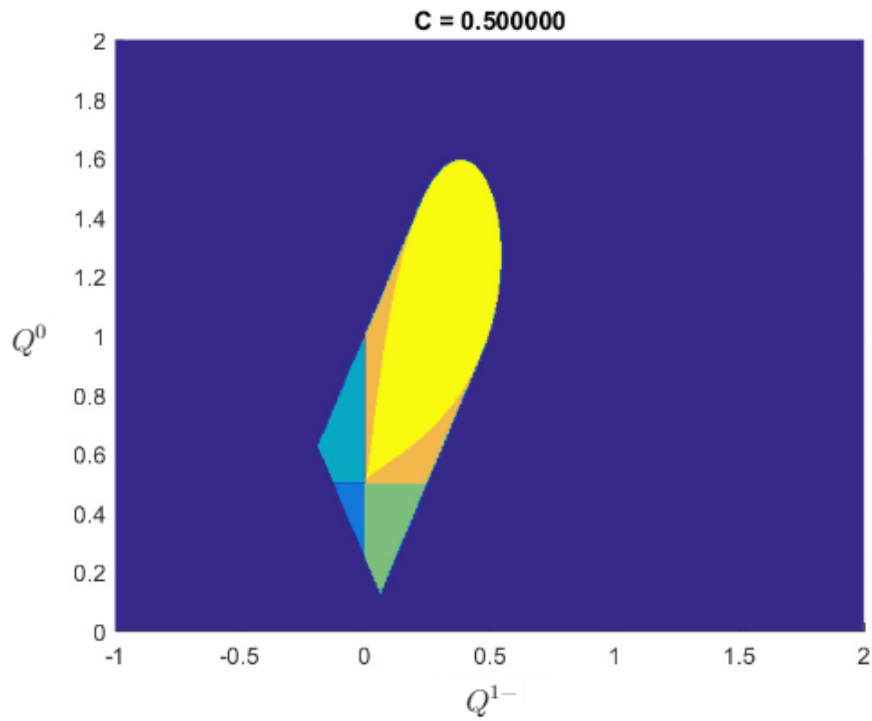
Figure 1: Linear stability map for $C = 0.5$ and $Q^{1+} = 0$.

1. Dark blue$\rightarrow$ Outside linear stability

2. Green $\rightarrow$ Case 1.

3. Light blue$\rightarrow$ Case 2.

4. Turquoise$\rightarrow$ Case 3.

5. Yellow$\rightarrow$ Case 4. (a)

6. Orange$\rightarrow$ Case 4. (b)
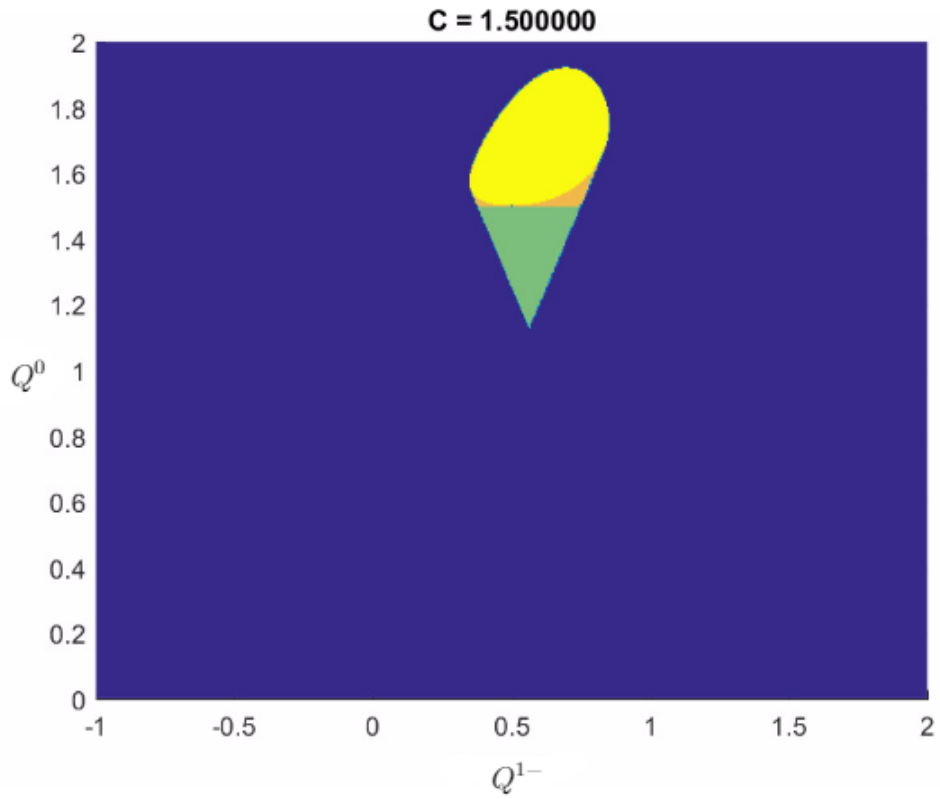
Figure 2: Linear stability map for $C = 1.5$ and $Q^{1+} = 0$.

1. Dark blue→ Outside linear stability

2. Green → Case 1.

3. Yellow→ Case 4. (a)

4. Orange→ Case 4. (b)

We continue with the more general expression (48), when $Q^{1+} \neq 0$ to see if there are some easy manipulations not yet discovered. The amplification factor is expressed in the same way

$$|g(z)|^2 = 1 - wA(w), \tag{54}$$

but this time $A(w)$ is a cubic polynomial

$$A(w) = a_3 w^3 + a_2 w^2 + a_1 w + a_0, \tag{55}$$

and the coefficients are:

1. $a_3 = 4q_1^2 - 4q_2^2$

2. $a_2 = 4q_1(Q^0 + 2q_1) - 4q_2(C + 2q_2)$

3. $a_1 = C^2 - (Q^0 + 2q_1)^2 + 4(2Cq_2 - q_1)$

4. $a_0 = 2(Q^0 + 2q_1 - C^2) = 2\sigma$

For simplicity we have written

$$q_1 = Q^{1-} + Q^{1+} \tag{56}$$

$$q_2 = Q^{1-} - Q^{1+} \tag{57}$$

The case $Q^{1+} = 0$ implies $q_1 = q_2$, and (55) reduces to (51). When $Q^{1+} \neq 0$ we can see that positive diffusion is required for linear stability, since $A(0)$ must be positive or zero. Both for the 3-point stencil and 5-point stencil we have shown that positive diffusion is a necessary condition for linear stability. We believe that this is also true for a general (2k+1)-point stencil, and one of the motivations for extending the von Neumann analysis to a general (2k+1)-point stencil is to give an algebraic proof of the conjecture.

3.1.2 (2k+1)-point scheme

The fluxes in the conservative formulation are expanded to cover a (2k+1)-point scheme

$$
\begin{aligned}
f_{j+1/2} = \frac{1}{2}(f_j + f_{j+1}) &- \frac{\Delta x}{2\Delta t}Q^0(\epsilon_{j+1} - \epsilon_j) \\
&- \frac{\Delta x}{\Delta t}\sum_{i=1}^{k-1}(Q^{i-}(\epsilon_{j-i+1} - \epsilon_{j-i}) + Q^{i+}(\epsilon_{j+i+1} - \epsilon_{j+i})).
\end{aligned}
\tag{58}
$$

The same procedure as for the 5-point stencil gives us the updated cell error value

17

$$
\begin{aligned}
\epsilon_j^{n+1} = {} & \epsilon_j^n - \frac{a\Delta t}{2\Delta x}(\epsilon_{j+1}^n - \epsilon_{j-1}^n) \\
& + \frac{1}{2}Q^0(\epsilon_{j+1}^n - 2\epsilon_j^n + \epsilon_{j-1}^n) \\
& + Q^{1-}(\epsilon_j^n - 2\epsilon_{j-1}^n + \epsilon_{j-2}^n) \\
& + Q^{1+}(\epsilon_{j+2}^n - 2\epsilon_{j+1}^n + \epsilon_j^n) \\
& \quad . \\
& \quad . \\
& \quad . \\
& + Q^{(k-1)-}(\epsilon_{j-(k-1)+1}^n - 2\epsilon_{j-(k-1)}^n + \epsilon_{j-(k-1)-1}^n) \\
& + Q^{(k-1)+}(\epsilon_{j+(k-1)+1}^n - 2\epsilon_{j+(k-1)}^n + \epsilon_{j+(k-1)-1}^n)
\end{aligned}
\tag{59}
$$

and the amplification factor

$$
\begin{aligned}
g(\bar{k}_m \Delta x) = {} & 1 - \frac{C}{2}(e^{i\bar{k}_m \Delta x} - e^{-i\bar{k}_m \Delta x}) \\
& + \frac{1}{2}Q^0(e^{i\bar{k}_m \Delta x} - 2 + e^{-i\bar{k}_m \Delta x}) \\
& + Q^{1-}(e^{i\bar{k}_m \Delta x} - 2 + e^{-i\bar{k}_m \Delta x})e^{-i\bar{k}_m \Delta x} \\
& + Q^{1+}(e^{i\bar{k}_m \Delta x} - 2 + e^{-i\bar{k}_m \Delta x})e^{i\bar{k}_m \Delta x} \\
& \quad . \\
& \quad . \\
& \quad . \\
& + Q^{(k-1)-}(e^{i\bar{k}_m \Delta x} - 2 + e^{-i\bar{k}_m \Delta x})e^{-(k-1)i\bar{k}_m \Delta x} \\
& + Q^{(k-1)+}(e^{i\bar{k}_m \Delta x} - 2 + e^{-i\bar{k}_m \Delta x})e^{(k-1)i\bar{k}_m \Delta x}.
\end{aligned}
\tag{60}
$$

For simplicity we let $z = \cos(\bar{k}_m \Delta x)$ and $y = \sin(\bar{k}_m \Delta x)$

$$
\begin{aligned}
g(y, z) = {} & 1 - Ciy \\
& + Q^0(z - 1) \\
& + 2Q^{1-}(z - 1)(z - iy) \\
& + 2Q^{1+}(z - 1)(z + iy) \\
& \quad . \\
& \quad . \\
& \quad . \\
& + 2Q^{(k-1)-}(z - 1)(z - iy)^{(k-1)} \\
& + 2Q^{(k-1)+}(z - 1)(z + iy)^{(k-1)}.
\end{aligned}
\tag{61}
$$

18

A general formula for a complex power is given in Abramowitz and Stegun [18]

$$
\begin{aligned}
(z+iy)^l &= \left[z^l - \binom{l}{2} z^{l-2}y^2 + \binom{l}{4} z^{l-4}y^4 - \ldots \right] \\
&\quad + i \left[\binom{l}{1} z^{l-1}y - \binom{l}{3} z^{l-3}y^3 + \ldots \right] \\
&= \left[z^l - \binom{l}{2} z^{l-2}y^2 + \binom{l}{4} z^{l-4}y^4 - \ldots \right] \\
&\quad + iy \left[\binom{l}{1} z^{l-1} - \binom{l}{3} z^{l-3}y^2 + \ldots \right] \\
&= g_l(y,z) + iyh_l(y,z)
\end{aligned}
\tag{62}
$$

$$
\begin{aligned}
(z-iy)^l &= \left[z^l - \binom{l}{2} z^{l-2}y^2 + \binom{l}{4} z^{l-4}y^4 - \ldots \right] \\
&\quad - i \left[\binom{l}{1} z^{l-1}y - \binom{l}{3} z^{l-3}y^3 + \ldots \right] \\
&= \left[z^l - \binom{l}{2} z^{l-2}y^2 + \binom{l}{4} z^{l-4}y^4 - \ldots \right] \\
&\quad - iy \left[\binom{l}{1} z^{l-1} - \binom{l}{3} z^{l-3}y^2 + \ldots \right] \\
&= g_l(y,z) - iyh_l(y,z),
\end{aligned}
\tag{63}
$$

where $l \in \{1, 2, 3, \ldots, (k-1)\}$. Inserting equation (62) and (63) into (61) gives

$$
\begin{aligned}
g(y,z) &= 1 + Q^0(z-1) \\
&\quad + 2(z-1) \sum_{l=1}^{k-1} (Q^{l-} + Q^{l+}) g_l(y,z) \\
&\quad - 2(z-1)iy \sum_{l=1}^{k-1} (Q^{l-} - Q^{l+}) h_l(y,z) \\
&\quad - Cyi \\
&= \left[1 + (z-1) \left(Q^0 + 2 \sum_{l=1}^{k-1} (Q^{l-} + Q^{l+}) g_l(y,z) \right) \right] \\
&\quad - iy \left[C + 2(z-1) \sum_{l=1}^{k-1} (Q^{l-} - Q^{l+}) h_l(y,z) \right]
\end{aligned}
\tag{64}
$$

For stability we need $|g| \le 1$. The amplification factor is in general a complex number, so we take the modulus of g squared.

19

$$|g|^2 = \left[1 + (z-1)\left(Q^0 + 2\sum_{l=1}^{k-1}(Q^{l-} + Q^{l+})g_l(y,z)\right)\right]^2$$

$$+ y^2 \left[C + 2(z-1)\sum_{l=1}^{k-1}(Q^{l-} - Q^{l+})h_l(y,z)\right]^2$$

$$= 1 - (1-z)\left[2\left(Q^0 + 2\sum_{l=1}^{k-1}(Q^{l-} + Q^{l+})g_l(y,z)\right)\right.$$

$$- (1-z)\left(Q^0 + 2\sum_{l=1}^{k-1}(Q^{l-} + Q^{l+})g_l(y,z)\right)^2$$

$$\left. -(1+z)\left(C + 2(z-1)\sum_{l=1}^{k-1}(Q^{l-} - Q^{l+})h_l(y,z)\right)^2\right] \qquad (65)$$

$$= 1 - (1-z)\left[2\left(Q^0 + 2\sum_{l=1}^{k-1}(Q^{l-} + Q^{l+})g_l(y,z)\right)\right.$$

$$- (1-z)\left(Q^0 + 2\sum_{l=1}^{k-1}(Q^{l-} + Q^{l+})g_l(y,z)\right)^2$$

$$+ (1-z)\left(C - 2(1-z)\sum_{l=1}^{k-1}(Q^{l-} - Q^{l+})h_l(y,z)\right)^2$$

$$\left. -2\left(C - 2(1-z)\sum_{l=1}^{k-1}(Q^{l-} - Q^{l+})h_l(y,z)\right)^2\right]$$

We want to write the equation in the form

$$|g|^2 = 1 - wA(w) \qquad (66)$$

Where $w = 1 - z$, $w \in [0,2]$ and $A(w)$ is a polynomial

$$A(w) = a_0 + a_1 w + a_2 w^2 + a_3 w^3 + ... \qquad (67)$$

If we can show that a_0 is proportional to the numerical diffusion σ, then we have proved that positive diffusion is a necessary condition for linear stability. To show this we need to take a further look at the term

$$Q^0 + 2\sum_{l=1}^{k-1}(Q^{l-} + Q^{l+})g_l(y,z), \qquad (68)$$

and rewrite $g_l(y,z)$ as a product of the factor $(1-z)$

$$g_l(y, z) = \left[z^l - \binom{l}{2} z^{l-2} y^2 + \binom{l}{4} z^{l-4} y^4 - \ldots \right]$$

$$= \left[z^l - 1 + 1 - \binom{l}{2} z^{l-2} y^2 + \binom{l}{4} z^{l-4} y^4 - \ldots \right]$$

$$= \left[-(1 - z)(z^{l-1} + z^{l-2} + \ldots z^2 + z + 1) + 1 - \binom{l}{2} z^{l-2} y^2 + \binom{l}{4} z^{l-4} y^4 - \ldots \right].$$
(69)

The remaining terms involving y will always be an even power of y. This allows us to factorise $y^2 = 1 - z^2 = (1 - z)(1 + z)$. All the terms are now a factor of $(1 - z)$ except for a constant term equal to 1.

$$g_l(y, z) = \left[-(1 - z)(z^{l-1} + z^{l-2} + \ldots z^2 + z + 1) + 1 - \binom{l}{2} z^{l-2} y^2 + \binom{l}{4} z^{l-4} y^4 - \ldots \right]$$

$$= 1 + (1 - z)\hat{g}_l(y, z)$$
(70)

where

$$\hat{g}_l(y, z) = -(z^{l-1} + z^{l-2} + \ldots z^2 + z + 1) - \binom{l}{2} z^{l-2}(1 + z) + \binom{l}{4} z^{l-4} y^2(1 + z) - \ldots \quad (71)$$

We return to the amplification factor (65) and use the above factorisation of $g_l(y, z)$.

$$|g|^2 = 1 - (1-z)\left[2\left(Q^0 + 2\sum_{l=1}^{k-1}(Q^{l-} + Q^{l+}) + 2(1-z)\sum_{l=1}^{k-1}(Q^{l-} + Q^{l+})\hat{g}_l(y,z)\right)\right.$$

$$- (1-z)\left(Q^0 + 2\sum_{l=1}^{k-1}(Q^{l-} + Q^{l+})g_l(y,z)\right)^2$$

$$+ (1-z)\left(C - 2(1-z)\sum_{l=1}^{k-1}(Q^{l-} - Q^{l+})h_l(y,z)\right)^2$$

$$\left. -2C^2 - 2(1-z)\left(-4C\sum_{l=1}^{k-1}(Q^{l-} - Q^{l+})h_l(y,z) + 4(1-z)\left(\sum_{l=1}^{k-1}(Q^{l-} - Q^{l+})h_l(y,z)\right)^2\right)\right]$$

$$= 1 - w\left[2\sigma + 4w\sum_{l=1}^{k-1}(Q^{l-} + Q^{l+})\hat{g}_l(y,z)\right.$$

$$- w\left(Q^0 + 2\sum_{l=1}^{k-1}(Q^{l-} + Q^{l+})g_l(y,z)\right)^2$$

$$+ w\left(C - 2w\sum_{l=1}^{k-1}(Q^{l-} - Q^{l+})h_l(y,z)\right)^2$$

$$\left. -2w\left(-4C\sum_{l=1}^{k-1}(Q^{l-} - Q^{l+})h_l(y,z) + 4w\left(\sum_{l=1}^{k-1}(Q^{l-} - Q^{l+})h_l(y,z)\right)^2\right)\right]$$

$$= 1 - wA(w) \tag{72}$$

Since $w = 1 - z$, $w \in [0, 2]$, a necessary condition is $A(w^+) > 0 \implies \sigma \geq 0$, by the arguments of continuity. We have in this section shown that linear stability implies positive or zero diffusion, with an algebraic poof. In practical implementation of a $(2k + 1)$-point LTS scheme we can use equation (61) to check for linear stability. In the next section we also want to connect the nonlinear TVD stability region (27)-(31), presented in section 2.3, with the linear stability region. In particular we want to confirm the statement:

• Non linear stability (TVD) implies linear stability for a $(2k + 1)$-point LTS scheme.

3.1.3 TVD implies linear stability

To prove the statement we use equation (61), but exchange the real variable z with the real variable x

$$g = 1 - Ciy$$
$$+ Q^0(x - 1)$$
$$+ 2Q^{1-}(x - 1)(x - iy)$$
$$+ 2Q^{1+}(x - 1)(x + iy)$$
$$.$$
$$.$$
$$.$$
$$+ 2Q^{(k-1)-}(x - 1)(x - iy)^{(k-1)}$$
$$+ 2Q^{(k-1)+}(x - 1)(x + iy)^{(k-1)},$$

where $x = \cos(\bar{k}_m \Delta x)$ and $y = \sin(\bar{k}_m \Delta x)$. Define the complex number z to be $z = x + iy$. In our case we have the following properties

1. $|z| = \sqrt{x^2 + y^2} = 1$

2. $\bar{z} = z^{-1}|z|^2 = z^{-1}$

3. $|\bar{z}| = \sqrt{x^2 + (-y)^2} = 1$

4. $x = \Re(z) = \frac{z + \bar{z}}{2} = \frac{z + z^{-1}}{2}$

5. $y = \Im(z) = \frac{z - \bar{z}}{2i} = \frac{z - z^{-1}}{2i}$

Rearranging equation (73) with the complex variable z

$$g = 1 - \frac{C}{2}(z - z^{-1}) + \frac{Q^0}{2}(z + z^{-1} - 2) + Q^{1-}(z + z^{-1} - 2)z^{-1} + Q^{1+}(z + z^{-1} - 2)z$$

$$+ Q^{2-}(z + z^{-1} - 2)z^{-2} + Q^{2+}(z + z^{-1} - 2)z^2 + \sum_{j=3}^{k-1}(z + z^{-1} - 2)(Q^{j-}z^{-j} + Q^{j+}z^j)$$

$$= 1 - Q^0 + Q^{1-} + Q^{1+} + \frac{1}{2}(Q^0 - 4Q^{1-} + 2Q^{2-} + C)z^{-1} + \frac{1}{2}(Q^0 - 4Q^{1+} + 2Q^{2+} - C)z$$

$$+ \sum_{j=1}^{k-1}(Q^{j-} - 2Q^{(j+1)-} + Q^{(j+2)-})z^{-(j+1)} + \sum_{j=1}^{k-1}(Q^{j+} - 2Q^{(j+1)+} + Q^{(j+2)+})z^{j+1}$$

(74)

Applying the triangle inequality on the amplification factor gives

$$|g| \leq \left|1 - Q^0 + Q^{1-} + Q^{1+}\right| + \left|\frac{1}{2}(Q^0 - 4Q^{1-} + 2Q^{2-} + C)z^{-1}\right| + \left|\frac{1}{2}(Q^0 - 4Q^{1+} + 2Q^{2+} - C)z\right|$$

$$+ \sum_{j=1}^{k-1}\left|(Q^{j-} - 2Q^{(j+1)-} + Q^{(j+2)-})z^{-(j+1)}\right| + \sum_{j=1}^{k-1}\left|(Q^{j+} - 2Q^{(j+1)+} + Q^{(j+2)+})z^{j+1}\right|$$

(75)

Since $\left| z^l \right| = 1 \quad \forall l$ we can cancel all powers of z.

$$|g| \leq \left| 1 - Q^0 + Q^{1-} + Q^{1+} \right| + \left| \frac{1}{2}(Q^0 - 4Q^{1-} + 2Q^{2-} + C) \right| + \left| \frac{1}{2}(Q^0 - 4Q^{1+} + 2Q^{2+} - C) \right|$$
$$+ \sum_{j=1}^{k-1} \left| (Q^{j-} - 2Q^{(j+1)-} + Q^{(j+2)-}) \right| + \sum_{j=1}^{k-1} \left| (Q^{j+} - 2Q^{(j+1)+} + Q^{(j+2)+}) \right| \tag{76}$$

We are now left with a number of expressions inside absolute value signs. From [1] we state the TVD conditions (27)-(31) in conservative form

$$1 - Q^0 + Q^{1-} + Q^{1+} \geq 0 \tag{77}$$

$$Q^0 - 4Q^{1\pm} + 2Q^{2\pm} \mp C \geq 0 \tag{78}$$

$$Q^{i\pm} - 2Q^{(i+1)\pm} + Q^{(i+2)\pm} \geq 0 \quad \forall i \geq 1 \tag{79}$$

If we say that every expression in (76) is greater or equal to zero, which would be equivalent to imposing the TVD conditions (77)-(79), we can remove the absolute value sign, and the complete expression nicely reduces to

$$|g| \leq 1. \tag{80}$$

We conclude that TVD stability implies linear stability! Another way to interpret the proof is purely geometrical, since all the powers of the complex variable z live on the unit circle in the complex plane. Connecting the points with straight lines gives an inscribed convex polygon within the unit circle, so any convex combination of the powers results in a point inside this polygon. When we impose the TVD restriction (77)-(79), the coefficients in equation (74) create a convex combination of the powers of z, because the coefficients are positive and sum to 1. The convex combination gives a complex number with absolute value less than or equal 1, which completes the proof.

3.2 Modified equation

The modified equation is the PDE which our discretized scheme is solving. We find the modified equation by Taylor expanding all the terms of a smooth function $U(x,t)$ inserted into the discrete equation around (x_j, t_n) up to desired order. The LTS schemes can be designed with higher order accuracy, if we carefully adjust the coefficients, in a way that leads to cancellation of terms in the modified equation. If our numerical schemes are consistent and stable, they will converge to the original PDE. First we find the modified equation for a linear (2k+1)-point large time step scheme up to third order. The coefficients $\mathcal{A}_{j\mp1/2\mp i}^{i\pm}$ are constant in this case.

24

3.2.1 Linear equation

A general Large time step scheme in the flux difference splitting formulation is given by

$$U_j^{n+1} = U_j^n - \sum_{i=0}^{k-1} \left(\mathcal{A}_{j-1/2-i}^{i+} \Delta_{j-1/2-i} + \mathcal{A}_{j+1/2+i}^{i-} \Delta_{j+1/2+i} \right) \tag{81}$$

where

$$\Delta_{j+1/2} = U_{j+1}^n - U_j^n \tag{82}$$

Taylor expanding $U(x_j, t_{n+1})$ and $U(x_{j+i}, t_n)$, where $i \in \{-k, ..., -2, -1, 1, 2, ..., k\}$ around (x_j, t_n) gives the following

$$U_j^{n+1} = U + \Delta t U_t + \frac{\Delta t^2}{2} U_{tt} + \frac{\Delta t^3}{3!} U_{ttt} + \mathcal{O}(\Delta t^4) \tag{83}$$

$$U_{j-i} = U_j - i\Delta x U_x + \frac{(i\Delta x)^2}{2} U_{xx} - \frac{(i\Delta x)^3}{3!} U_{xxx} + \mathcal{O}(\Delta x^4) \tag{84}$$

$$U_{j-(i+1)} = U_j - (i+1)\Delta x U_x + \frac{((i+1)\Delta x)^2}{2} U_{xx} - \frac{((i+1)\Delta x)^3}{3!} U_{xxx} + \mathcal{O}(\Delta x^4) \tag{85}$$

$$\begin{aligned} \Delta_{j-1/2-i} &= U_{j-i}^n - U_{j-(i+1)}^n \\ &= \Delta x U_x - \frac{\Delta x^2}{2}(2i+1)U_{xx} + \frac{\Delta x^3}{3!}(3i^2 + 3i + 1)U_{xxx} + \mathcal{O}(\Delta x^4) \end{aligned} \tag{86}$$

$$\begin{aligned} \Delta_{j+1/2+i} &= U_{j+i+1}^n - U_{j+i}^n \\ &= \Delta x U_x + \frac{\Delta x^2}{2}(2i+1)U_{xx} + \frac{\Delta x^3}{3!}(3i^2 + 3i + 1)U_{xxx} + \mathcal{O}(\Delta x^4) \end{aligned} \tag{87}$$

Insert (83),(86) and (87) into (81) gives to third order

$$\begin{aligned} U_t + \frac{\Delta x}{\Delta t}\sum_{i=0}^{k-1}\left(\mathcal{A}^{i+} + \mathcal{A}^{i-}\right)U_x =& \frac{\Delta x^2}{2\Delta t}\sum_{i=0}^{k-1}(2i+1)\left(\mathcal{A}^{i+} - \mathcal{A}^{i-}\right)U_{xx} \\ &- \frac{\Delta x^3}{3!\Delta t}\sum_{i=0}^{k-1}(3i^2 + 3i + 1)\left(\mathcal{A}^{i+} + \mathcal{A}^{i-}\right)U_{xxx} \\ &- \frac{\Delta t}{2}U_{tt} - \frac{\Delta t^2}{3!}U_{ttt} + \mathcal{O}(\Delta x^3, \Delta t^3) \end{aligned} \tag{88}$$

Next we want to change the higher order time derivatives to space derivatives. We take the following partial derivatives $\frac{\partial}{\partial t}$, $\frac{\partial^2}{\partial t^2}$, $\frac{\partial^2}{\partial t\partial x}$, $\frac{\partial}{\partial x}$ and $\frac{\partial^2}{\partial x^2}$ of equation (88) $U_t + \bar{a}U_x = \bar{b}U_{xx} + \bar{c}U_{xxx} + \bar{d}U_{tt} + \bar{e}U_{ttt} + \mathcal{O}(\Delta x^3, \Delta t^3)$, with the following constants

- $\bar{a} = \frac{\Delta x}{\Delta t} \sum_{i=0}^{k-1} \left(\mathcal{A}^{i+} + \mathcal{A}^{i-} \right)$

- $\bar{b} = \frac{\Delta x^2}{2\Delta t} \sum_{i=0}^{k-1} (2i+1) \left(\mathcal{A}^{i+} - \mathcal{A}^{i-} \right)$

- $\bar{c} = -\frac{\Delta x^3}{3!\Delta t} \sum_{i=0}^{k-1} (3i^2 + 3i + 1) \left(\mathcal{A}^{i+} + \mathcal{A}^{i-} \right)$

- $\bar{d} = -\frac{\Delta t}{2}$

- $\bar{e} = -\frac{\Delta t^2}{3!}$

leads to

- $\frac{\partial}{\partial t}:$ $U_{tt} + \bar{a} U_{xt} = \bar{b} U_{xxt} + \bar{d} U_{ttt} + \mathcal{O}(\Delta x^2, \Delta t^2)$

- $\frac{\partial^2}{\partial t^2}:$ $U_{ttt} + \bar{a} U_{xtt} = \mathcal{O}(\Delta x, \Delta t)$

- $\frac{\partial^2}{\partial t \partial x}:$ $U_{ttx} + \bar{a} U_{xxt} = +\mathcal{O}(\Delta x, \Delta t)$

- $\frac{\partial}{\partial x}:$ $U_{tx} + \bar{a} U_{xx} = \bar{b} U_{xxx} + \bar{d} U_{ttx} + \mathcal{O}(\Delta x^2, \Delta t^2)$

- $\frac{\partial^2}{\partial x^2}:$ $U_{txx} + \bar{a} U_{xxx} = +\mathcal{O}(\Delta x, \Delta t)$

Bringing all together into the modified equation gives

$$U_t + \bar{a} U_x = (\bar{b} + \bar{a}^2 \bar{d}) U_{xx} + (\bar{c} - 2\bar{a}\bar{b}\bar{d} - 2\bar{a}^3 \bar{d}^2 - \bar{a}^3 \bar{e}) U_{xxx} + \mathcal{O}(\Delta x^3, \Delta t^3), \qquad (89)$$

Δt behaves as Δx due to the constant Courant number, and we write $\mathcal{O}(\Delta x^3, \Delta t^3) = \mathcal{O}(\Delta x^3)$. Finally we write out the complete expression

$$U_t + \frac{\Delta x}{\Delta t} \sum_{i=0}^{k-1} \left(\mathcal{A}^{i+} + \mathcal{A}^{i-} \right) U_x = \frac{\Delta x^2}{2\Delta t} \left(\sum_{i=0}^{k-1} (2i+1) \left(\mathcal{A}^{i+} - \mathcal{A}^{i-} \right) - C^2 \right) U_{xx}$$

$$+ \frac{\Delta x^3}{6\Delta t} \left(3C \sum_{i=0}^{k-1} (2i+1) \left(\mathcal{A}^{i+} - \mathcal{A}^{i-} \right) - \sum_{i=0}^{k-1} (3i^2 + 3i + 1) \left(\mathcal{A}^{i+} + \mathcal{A}^{i-} \right) - 2C^3 \right) U_{xxx} + \mathcal{O}(\Delta x^3).$$

$$(90)$$

26

3.2.2 Nonlinear equation

The difference for the non linear modified equation is that the coefficients $\mathcal{A}^{i\pm}_{j\mp 1/2\mp i}\left(C^{i\pm}_{j\mp 1/2\mp i}\right)$ now depend on the local cell face Courant number. So this must be taken into account when we do Taylor expansion. A complete derivation is given in [12] up to second order, here we just state the result

$$U_t + \frac{\Delta x}{\Delta t}\sum_{i=0}^{k-1}\left(\mathcal{A}^{i+} + \mathcal{A}^{i-}\right)U_x = \frac{\Delta x^2}{2\Delta t}\partial_x\left(\sum_{i=0}^{k-1}(2i+1)\left(\mathcal{A}^{i+} - \mathcal{A}^{i-}\right) - C^2\right)U_x + \mathcal{O}(\Delta x^2). \tag{91}$$

This is equivalent to the linear modified equation up to second order. But this shows that it is also applicable to nonlinear advection equations

$$\frac{\partial u}{\partial t} + f'(u)\frac{\partial u}{\partial x} = 0. \tag{92}$$

4 Construction of new LTS schemes

There are two goals we want to reach throughout this chapter. First we would like to create a robust oscillation-free LTS scheme for hyperbolic systems of conservation laws, not caring too much about accuracy. Second we explore the possibility of expanding the LTS method to include parabolic partial differential equations by carefully manipulating terms in the modified equation.

4.1 Design framework for LTS schemes

A motivation for introducing an alternative formulation for the LTS coefficients is a more practical way to design new numerical schemes with desired properties. The LTS Roe and the LTS Lax-Friedrichs schemes were constructed as TVD schemes with minimum and maximum numerical diffusion respectively. A convex combination of the two schemes creates a new TVD scheme, with the ability of containing an amount of numerical diffusion spanned by the two extreme cases. The scheme is referred to as the **LTS β scheme**. The coefficients of the flux-difference splitting form (23) are defined by

$$\mathcal{A}^{i\pm} = \beta\mathcal{A}^{i\pm}_{\text{LF}} + (1-\beta)\mathcal{A}^{i\pm}_{\text{Roe}}, \tag{93}$$

where $\mathcal{A}^{i\pm}_{\text{LF}}$ and $\mathcal{A}^{i\pm}_{\text{Roe}}$ are the coefficients defined in (37) and (35)-(36), respectively. The parameter $\beta \in [0,1]$ gives the LTS Roe scheme when $\beta = 0$ and the LTS Lax-Friedrichs scheme when $\beta = 1$. Even though all possible values of diffusion in the TVD range can be reproduced by the LTS β scheme, it does not span the entire domain of TVD LTS schemes. LTS schemes with a given amount of numerical diffusion are not necessarily unique.

We introduce a new function $a(i,C)$, which is used to determine the LTS coefficients $\mathcal{A}^{i\pm}$ in the flux-difference splitting formulation. The function is an approximate solution to the cell interface Riemann problem scaled with $\Delta t/\Delta x$. $C = \frac{\Delta t}{\Delta x}f'(u)$ is the local Courant number. We find the coefficients $\mathcal{A}^{i\pm}$ by integrating over the corresponding cell

$$\mathcal{A}^{i+} = \int_i^{i+1} a(\zeta, C)\mathrm{d}\zeta \tag{94}$$

$$\mathcal{A}^{i-} = \int_{-(i+1)}^{-i} a(\zeta, C)\mathrm{d}\zeta - 1 \tag{95}$$

Notice that we subtract the integral by 1 in equation (95). With this convention we avoid a jump in the function $a(i,C)$ at $i = 0$. We can interpret the coefficients $\mathcal{A}^{i\pm}$ as a finite volume representation of the continuous function $a(i,C)$ and $a(i,C) - 1$ respectively. $\mathcal{A}^{i\pm}$ are a set of discrete numbers. Immediately we see that $a(i,C)$ does not uniquely determine $\mathcal{A}^{i\pm}$, because we can always change the function so that the integral stays the same. The function is graphed for a 11-point stencil in figure 3. A sufficient
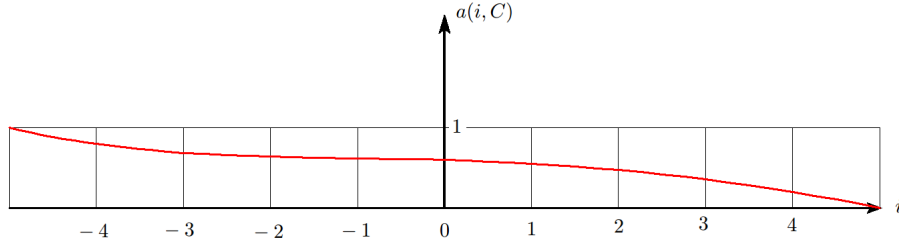
Figure 3: The function $a(i, C)$ graphed for a 11-point stencil

condition for TVD is for the function $a(i, C)$ to lie in the interval $0 \leq a(i, C) \leq 1$ and at the same time $a(i, C)$ is a nonincreasing function. The condition follows from the TVD conditions (27)-(31).

Next we show how the function $a(i, C)$ relates to the familiar LTS Roe, Lax-Friedrichs and β schemes, and give explicit formulas for them. We construct functions that obey the condition for TVD. For the LTS Roe scheme we give the function

$$a(i, C) = \begin{cases} 1 & \text{if} \quad i < C \\ 0 & \text{if} \quad i > C \end{cases} \tag{96}$$

This function reflects the nature of LTS Roe in the way that it is the "sharpest" TVD scheme. By "sharpest" we mean that everything behind the propagating discontinuity is fully affected and nothing ahead, except inside the cell corresponding to the local Courant number.
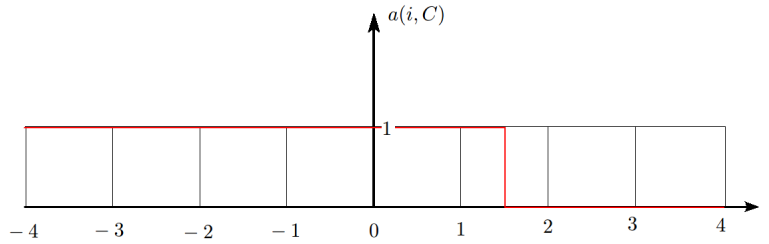
Figure 4: The function $a(i, C)$ representing the LTS Roe scheme for a 9-point stencil with $C = 1.5$

For the LTS Lax-Friedrichs scheme we have a constant $a(i, C)$ function

$$a(i, C) = \frac{1}{2k}(k + C). \tag{97}$$

The number k determines the stencil width according to the (2k+1)-point stencil formula. Changing C within the allowed interval $-k \leq C \leq k$ moves the constant function $a(i, C)$ between 0 and 1. In the extreme cases $C = \pm k$, the LTS Lax-Friedrichs

29

scheme is equal to the LTS Roe scheme. An example is shown in figure 5. We choose $C = 1.5$ for a 9-point stencil, then the constant $a(i, C) = \frac{1}{8}(1.5 + 4) = \frac{11}{16}$.
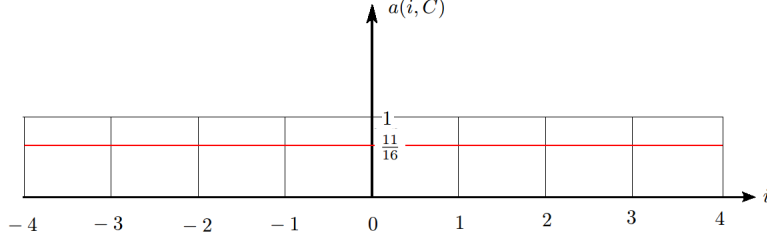
Figure 5: The function $a(i, C)$ representing the LTS Lax-Friedrichs scheme for a 9-point stencil with $C = 1.5$

From the two above schemes we can now define an $a(i, C)$ function for the LTS β scheme.

$$a(i, C) = (1 - \beta)a(i, C)^{\text{LTS Roe}} + \beta a(i, C)^{\text{LTS LxF}} \tag{98}$$

An illustration is provided in figure 6. Also this time we let $C = 1.5$ and $k = 4$. The parameter $1 - \beta$ quantifies the jump in the $a(i, C)$ function.
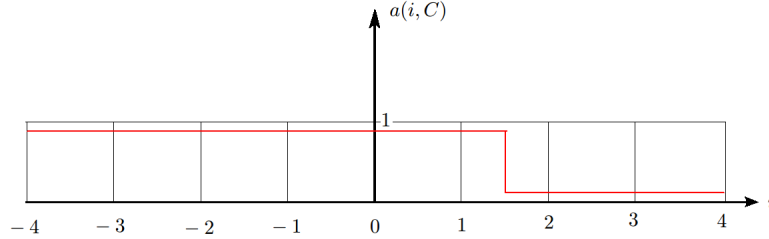
Figure 6: The function $a(i, C)$ representing the LTS β scheme for a 9-point stencil with $C = 1.5$ and $\beta = 0.1$

4.1.1 The $a(i, C)$ function

The $a(i, C)$ function is an approximate solution to the cell interface Riemann problem scaled with $\Delta t / \Delta x$. With the LTS Roe the a-function is the original discontinuity only translated a distance equal to the local Courant number, and can be interpreted as pure convection with no loss of information, except when we hit inside a cell $C \notin \mathbb{Z}$ and average the function with the operator (94) or (95). Then the discrete distribution no longer corresponds to the continuous distribution, and we have a diffusive effect with

loss of information. Only for Courant numbers $C \in \mathbb{Z}$, the discrete distribution matches the continuous distribution, and no diffusion is introduced.

Say we split the discontinuity into two and send the lower part to the right end of the stencil and the upper part to the left end of the stencil, then we have the LTS Lax-Friedrich a-function, see figure 7. The dividing point is obtained from (97). Information is thus scattered all over the computational domain and yields a very diffusive scheme.

In the same way we think of the LTS β scheme as a discontinuity divided into three parts, where the lower and upper part are propagated to the right and left end of the stencil, respectively. The middle part is convected corresponding to the Courant number, see figure 8. The dividing points are now determined by (98). In this numerical scheme the parameter β tunes how much information that is convected exactly and how much information is scattered.
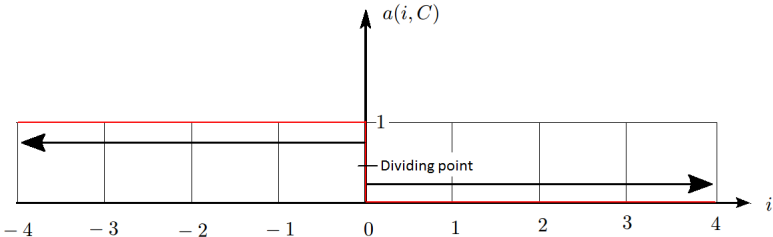
Figure 7: Interpretation of the function $a(i, C)$ for the LTS Lax-Friedrichs scheme.
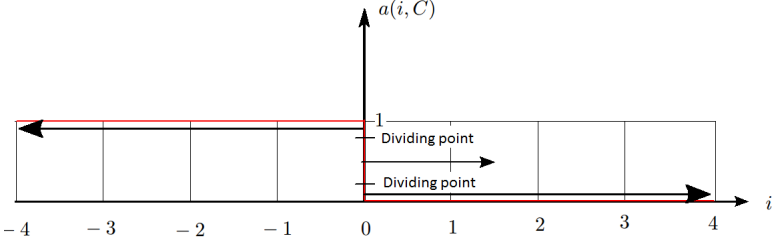
Figure 8: Interpretation of the function $a(i, C)$ for the LTS β scheme.

4.2 The LTS CD$\hat{k}$ schemes

We will now use this framework to design new LTS schemes by constructing a convenient function $a(i, C)$. A first thought is to minimize the jump in the LTS Roe function. This is also a consequence of the introduction of the LTS β scheme, but since it is a linear combination of the LTS Roe scheme and the LTS Lax-Friedrichs scheme it will change all the cells in a stencil. We want to affect the neighbouring cells around

the cell corresponding to the local Courant number C and at the same time reduce the jump. As a first step we smear the discontinuity symmetrically over an interval of $i \in [C-1, C+1]$. The smearing is represented by a linear function over the interval. We denote the scheme as **LTS Constant-Diffusion-1 (LTS CD1)**. A central property of the scheme is that the diffusion coefficient $\sigma(C)$, apparent in the modified equation given by Bore [12], is independent of the Courant number. A formula for the $a(i, C)$ function in this case is

$$a(i, C) = \begin{cases} 1 & \text{if} \quad i < C - 1 \\ \frac{1}{2}(C - i) + \frac{1}{2} & \text{if} \quad C - 1 < i < C + 1 \\ 0 & \text{if} \quad i > C + 1 \end{cases} \tag{99}$$

For this scheme we need to extend our stencil by 1, hence the number 1 in the name, because of the symmetrical smearing. The function will always distort cells exactly one cell ahead of the Courant number. We use (94) and (95) to compute the coefficients, and insert them into the formula for the diffusion coefficient.

$$\sigma(C) = \sum_{i=0}^{k} (2i + 1)(\mathcal{A}^{i+} - \mathcal{A}^{i-}) - C^2 = \frac{1}{2} \tag{100}$$
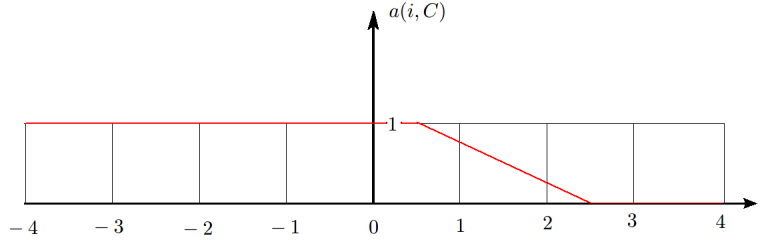
Figure 9: The function $a(i, C)$ representing the LTS CD1 scheme for a 9-point stencil with $C = 1.5$

This reveals an interesting property of the scheme. The diffusion coefficient is now dependent on another parameter, the smearing interval, not the local Courant number. To see this we expand the idea and extend the interval to $i \in [C-2, C+2]$. The scheme is now referred to as the **LTS CD2**. The $a(i, C)$ function then becomes

$$a(i, C) = \begin{cases} 1 & \text{if} \quad i < C - 2 \\ \frac{1}{4}(C - i) + \frac{1}{2} & \text{if} \quad C - 2 < i < C + 2 \\ 0 & \text{if} \quad i > C + 2 \end{cases} \tag{101}$$

and the stencil is increased by 2 compared to the original scheme with the same Courant number. In the same way we compute the numerical diffusion coefficient $\sigma(C) = \frac{3}{2}$ and observe the same constant behavior. Inspired by the results we try to find a relationship between the numerical diffusion coefficient and the smearing interval.
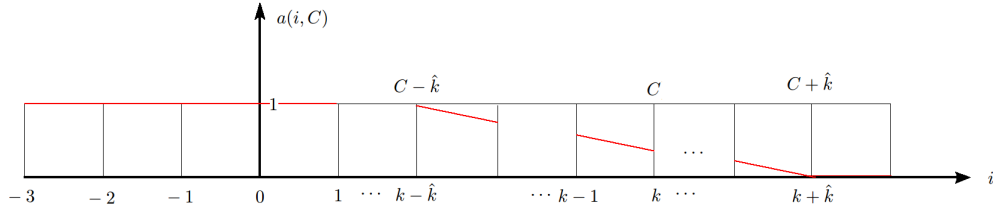
Figure 10: The function $a(i,C)$ representing the LTS CD$\hat{k}$ scheme for a $(2(k+\hat{k})+1)$-point stencil with $C = k$.

We look at a general **LTS CD$\hat{k}$** scheme, $\hat{k} \in \{1, 2, 3, ...\}$, for which the function $a(i,C)$ is illustrated in figure 10. The smearing interval is now $i \in [C - \hat{k}, C + \hat{k}]$, and we need an equivalent length of the numerical stencil $(2(\text{k}+\hat{k})+1)$. The $a(i,C)$ function is given by

$$a(i,C) = \begin{cases} 1 & \text{if} \quad i < C - \hat{k} \\ \frac{1}{2\hat{k}}(C - i) + \frac{1}{2} & \text{if} \quad C - \hat{k} < i < C + \hat{k} \\ 0 & \text{if} \quad i > C + \hat{k} \end{cases} \tag{102}$$

The diffusion coefficient is now computed to be

$$\sigma(C) = \sum_{i=0}^{k-1+\hat{k}} (2i + 1)(\mathcal{A}^{i+} - \mathcal{A}^{i-}) - C^2 = \frac{2\hat{k}^2 + 1}{6}. \tag{103}$$

We do a quick sanity check to validate the formula, setting $\hat{k}$ equal to 1 and 2, and the formula gives the correct values corresponding to the introducing cases. The diffusion coefficient is a quadratic function of the smearing interval $\hat{k}$. This family of TVD LTS schemes exhibits a robust way of adding numerical diffusion to the problem at hand. But for now the schemes only have discrete values for the diffusion coefficients. Some values are given in table 1. Observe that the diffusion coefficient increases with $\hat{k}$, which increases the smearing of the solution. We desire a continuous spectrum of numerical diffusion, therefore in the next section we will expand this method further to improve on this point.

Table 1: The first five values for the diffusion coefficient corresponding to the LTS CD$\hat{k}$ scheme.

$\hat{k}$	1	2	3	4	5
σ	$\frac{1}{2} = 0.50$	$\frac{3}{2} = 1.50$	$\frac{19}{6} = 3.17$	$\frac{11}{2} = 5.50$	$\frac{17}{2} = 8.50$

33

4.3 Extending the LTS CD$\hat{k}$ schemes

We pursue the same way of reasoning, when we extend our LTS CD$\hat{k}$ schemes, introducing a new parameter ϕ which gives an extra degree of freedom. The parameter ϕ is the slope of the $a(i, C)$ function located in the smearing interval. To ensure that the method is consistent [12]

$$\sum_{i=0}^{k-1+\hat{k}} (\mathcal{A}^{i+} + \mathcal{A}^{i-}) = C, \tag{104}$$

the $a(i, C)$ function must be given by

$$a(i, C) = \begin{cases} 1 & \text{if } i < C - \hat{k} \\ \phi(C - i) + \frac{1}{2} & \text{if } C - \hat{k} < i < C + \hat{k} \\ 0 & \text{if } i > C + \hat{k} \end{cases} \tag{105}$$

In the introduction we gave a sufficient condition for the $a(i, C)$ function to be TVD. The parameter ϕ lying in the interval $0 \leq \phi \leq \frac{1}{2\hat{k}}$ will satisfy this TVD condition. With this restriction on ϕ, the range of $a(C - \hat{k}, C)$ is $[0.5, 1]$ and the range of $a(C + \hat{k}, C)$ is $[0, 0.5]$. The interval $i \in [C - \hat{k}, C + \hat{k}]$ is connected by a linear function with a negative slope, thus the function $a(i, C)$ satisfies the TVD condition. We do the same analysis on these schemes as we did for the LTS CD$\hat{k}$ schemes and call them **LTS CD$\hat{k} - \phi$** schemes. We start off with the simplest cases when $\hat{k} = 1$ and $\hat{k} = 2$, and then move on to the general case. Figure 11 shows the function $a(i, C)$ for the LTS CD1-ϕ with $\phi > \frac{1}{2}$. Calculating the numerical diffusion coefficient results in

$$\sigma(C) = \sum_{i=0}^{k} (2i + 1)(\mathcal{A}^{i+} - \mathcal{A}^{i-}) - C^2 = 2\left(\phi - \frac{1}{2}\right)\left(\alpha^2 - \alpha - \frac{1}{2}\right) + \frac{1}{2}, \tag{106}$$

where $\alpha = \text{ceil}(C) - C$, $\alpha \in [0, 1]$ and the ceil function computes the nearest integer rounded up. As expected the expression reduces to the diffusion coefficient for the LTS CD1 scheme when $\phi = \frac{1}{2}$. But now the expression also depends on the local Courant number C. To achieve a constant diffusion we can use the one parameter freedom to adjust for the α dependence. Say that we want a diffusion coefficient $\sigma(C) = \sigma_0$, and then solve for the slope ϕ

$$\phi = \frac{\frac{1}{4} - \frac{\sigma_0}{2}}{\frac{1}{2} + \alpha - \alpha^2} + \frac{1}{2}. \tag{107}$$

Imposing the TVD condition

$$0 \leq \phi \leq \frac{1}{2}, \tag{108}$$

leads to an allowable diffusion interval for the LTS CD1-ϕ scheme

$$\frac{1}{2} \leq \sigma_0 \leq \frac{5}{4} \tag{109}$$
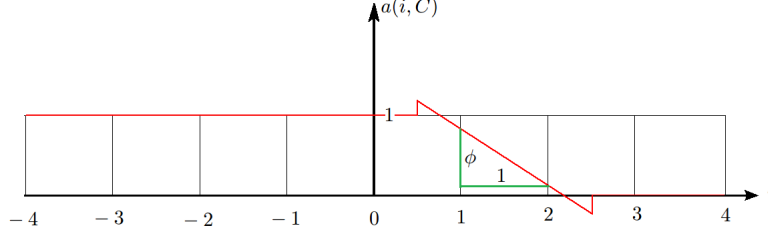
Figure 11: The function $a(i, C)$ representing the LTS CD1-ϕ scheme for a 9-point stencil with $C = 1.5$.

We continue with the case $\hat{k} = 2$ and do the same analysis. Figure 12 shows the function $a(i, C)$ for the LTS CD2 $- \phi$ scheme with $\phi > \frac{1}{4}$. Results are given below.

$$\sigma(C) = \sum_{i=0}^{k+1} (2i + 1)(\mathcal{A}^{i+} - \mathcal{A}^{i-}) - C^2 = 2\left(\phi - \frac{1}{4}\right)\left(2\alpha^2 - 2\alpha - 5\right) + \frac{3}{2}. \tag{110}$$

Solving for ϕ with a given diffusion coefficient σ_0 yields

$$\phi = \frac{\frac{3}{4} - \frac{\sigma_0}{2}}{5 + 2\alpha - \alpha^2} + \frac{1}{4}. \tag{111}$$

Imposing the TVD condition

$$0 \leq \phi \leq \frac{1}{4}, \tag{112}$$

leads to an allowable diffusion interval for the LTS CD2-ϕ scheme

$$\frac{3}{2} \leq \sigma_0 \leq \frac{17}{4}. \tag{113}$$

We observe from the range of the allowable diffusion, assuming TVD, that there exists a gap between the diffusion intervals. The maximum amount of diffusion for the LTS CD1-ϕ scheme is $\frac{5}{4}$ and the minimum amount of diffusion for the LTS CD2-ϕ scheme is $\frac{3}{2}$, leading to an interval of diffusion $[\frac{5}{4}, \frac{3}{2}]$ not covered. For robustness, we would like a numerical scheme able to span the entire domain of possible diffusion. When we move on to the general case, we will see if there are such gaps between all the discrete values of $\hat{k}$.

The function $a(i, C)$ for the LTS CD$\hat{k} - \phi$ scheme is illustrated in figure 13, and the general formula for the diffusion coefficient is given by
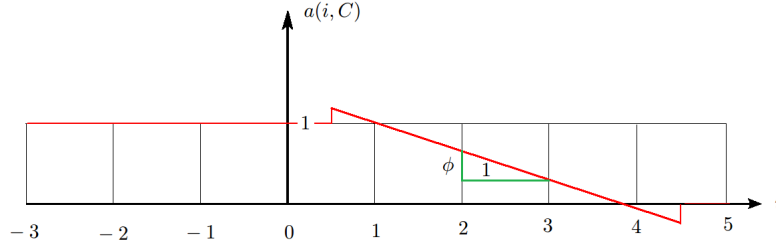
Figure 12: The function $a(i, C)$ representing the LTS CD2-ϕ scheme for a 9-point stencil with $C = 2.5$.

$$\sigma(C) = 2\left(\phi - \frac{1}{2\hat{k}}\right)\left(\alpha^2 - \alpha + \frac{1 - 4\hat{k}^2}{6}\right)\hat{k} + \frac{2\hat{k}^2 + 1}{6}. \tag{114}$$

Solving for ϕ

$$\phi = \frac{\frac{\sigma_0}{2} - \frac{2\hat{k}^2 + 1}{12}}{\hat{k}\left(\alpha^2 - \alpha + \frac{1 - 4\hat{k}^2}{6}\right)} + \frac{1}{2\hat{k}}, \tag{115}$$

and imposing the TVD conditions

$$0 \le \phi \le \frac{1}{2\hat{k}}, \tag{116}$$

leads to an allowable diffusion interval for the LTS CD$\hat{k} - \phi$ scheme

$$\frac{2\hat{k}^2 + 1}{6} \le \sigma_0 \le \frac{4\hat{k}^2 + 1}{4}. \tag{117}$$
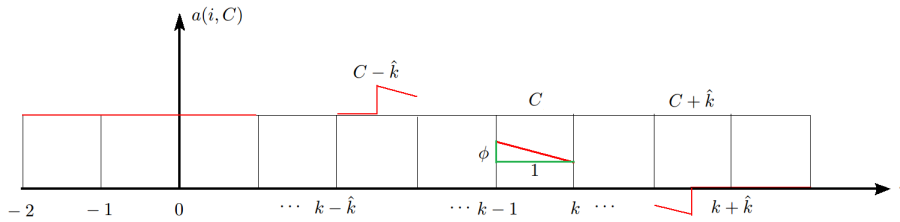

Figure 13: The function $a(i, C)$ representing the LTS CD$\hat{k}$-ϕ scheme for a $(2(k+\hat{k})+1)$-point stencil with $C = k - \frac{1}{2}$.

Now let us compare the maximum allowable diffusion of the LTS CD$\hat{k} - \phi$ with the minimum allowable diffusion of the LTS CD$(\hat{k} + 1) - \phi$ scheme. We want to find the

36

lowest $\hat{k}$, which closes the gaps between the discrete schemes. Consider the quadratic inequality

$$\frac{4\hat{k}^2 + 1}{4} > \frac{2(\hat{k}+1)^2 + 1}{6}, \tag{118}$$

which is true when $\hat{k} < \frac{1-\sqrt{\frac{5}{2}}}{2}$ or $\hat{k} > \frac{1+\sqrt{\frac{5}{2}}}{2}$. Only positive values of $\hat{k}$ are relevant for our analysis, so the LTS CD$\hat{k} - \phi$ TVD schemes with a $\hat{k} \geq 2$ spans a continuous range of numerical diffusion coefficients starting from $\frac{3}{2}$.

4.4   Second order LTS CD$\hat{k} - \phi$ schemes

In the previous section we considered LTS CD$\hat{k} - \phi$ schemes, which fulfilled the TVD condition. The schemes where only first order accurate because of numerical diffusion. A violation of the TVD condition allows us to increase the slope ϕ above $\phi = \frac{1}{2\hat{k}}$, pushing the diffusion coefficient σ_0 to $\sigma_0 = 0$, and achieving a second order accurate LTS scheme, denoted **LTS CD$\hat{k} - \phi - 2$**. Even though the LTS CD$\hat{k} - \phi - 2$ schemes no longer satisfy the strict nonlinear TVD stability criterion, they can still be linearly stable. A von Neumann analysis will tell, if they are linearly stable or not. Since we do not have a set of inequalities to describe the region of linear stability for a $(2(k+\hat{k})+1)$-point stencil, we must check each scheme with a combination of k and $\hat{k}$, by plugging the coefficients into the expression for the amplification factor given by (61).

4.5   Higher order LTS schemes

We propose a method for designing higher order LTS schemes, based on the second order scheme. Within the same interval $i \in [C - \hat{k}, C + \hat{k}]$ we replace the linear function in figure 13 by a $(p-1)$th order polynomial, which results in a pth order LTS scheme, if the polynomial coefficients are chosen properly. We determine the coefficients of the polynomial in such a way that the error terms in the modified equation cancel

$$U_t + a_1 U_x = \sum_{l=2}^{p} a_l \frac{\partial^l U}{\partial x^l} + \mathcal{O}(\Delta x^p), \tag{119}$$

where $a_1 = f'(u)$ and $a_l = 0, l = 2, ..., p$. This leads to solving a system of p linear algebraic equations. The first equation is for consistency, while the others equations remove numerical errors up to pth order. A numerical convergence analysis is performed in chapter 5, for a third order LTS scheme applied on the linear advection equation, with coefficients computed from the modified equation (90) derived in section 3.2.1

$$\frac{\Delta x}{\Delta t} \sum_{i=0}^{k-1+\hat{k}} \left(\mathcal{A}^{i+} + \mathcal{A}^{i-} \right) = a_1 \tag{120}$$

37

$$\frac{\Delta x^2}{2\Delta t}\left(\sum_{i=0}^{k-1+\hat{k}}(2i+1)\left(\mathcal{A}^{i+}-\mathcal{A}^{i-}\right)-C^2\right)=0 \tag{121}$$

$$\frac{\Delta x^3}{6\Delta t}\left(3C\sum_{i=0}^{k-1+\hat{k}}(2i+1)\left(\mathcal{A}^{i+}-\mathcal{A}^{i-}\right)-\sum_{i=0}^{k-1}(3i^2+3i+1)\left(\mathcal{A}^{i+}+\mathcal{A}^{i-}\right)-2C^3\right)=0 \tag{122}$$

4.6 Convection-diffusion equation

In this section we expand our idea of large time step methods to parabolic PDEs. We start with the simplest equation, the 1-dimensional convection-diffusion equation with constants coefficients

$$\frac{\partial u}{\partial t}+a\frac{\partial u}{\partial x}=\nu\frac{\partial^2 u}{\partial x^2}, \tag{123}$$

where a is the advection velocity and ν the viscosity. We would like to solve the problem with the LTS CD$\hat{k}-\phi$ schemes, originally developed for the advection equation. The LTS CD$\hat{k}-\phi$ schemes are consistent with the advection equation, and can therefore not be used directly. From the modified equation, we find that the fraction $\frac{\Delta x^2}{\Delta t}\to 0$, and the second order spatial derivative vanishes in the limit. A consistent numerical scheme for the convection-diffusion equation needs consistency between the numerical and physical diffusion. The numerical diffusion is the coefficient in front of the spatial second derivative in the modified equation (90)

$$\frac{\Delta x^2}{2\Delta t}\left(\sum_{i=0}^{k-1+\hat{k}}(2i+1)\left(\mathcal{A}^{i+}-\mathcal{A}^{i-}\right)-C^2\right)=\frac{\Delta x^2}{2\Delta t}\sigma=\nu \tag{124}$$

To fulfill this constraint we use a time step Δt of order $\mathcal{O}(\Delta x^2)$ so that the fraction does not vanish in the limit. As a consequence, the Courant number C is of order $\mathcal{O}(\Delta x)$. Solving equation (124) for σ and imposing the upper bound on σ according to the LTS CD$\hat{k}-\phi$ schemes gives the following inequality

$$\sigma=\frac{2\nu\Delta t}{\Delta x^2}\leq\hat{k}^2+\frac{1}{4}\quad\implies\quad\Delta t\leq\frac{\Delta x^2\left(\hat{k}^2+\frac{1}{4}\right)}{2\nu} \tag{125}$$

A traditional 3-point explicit numerical scheme for diffusion problems has a stability time step restriction equal $\Delta t\leq\frac{\Delta x^2}{2\nu}$, which closely coincides with our relaxed time step restrictions when $\hat{k}=1$. The relaxed time step increases with order $\mathcal{O}(\hat{k}^2)$, and at the same time the computational stencil increases with order $\mathcal{O}(\hat{k})$. So with fewer time steps more computational work is required in each time step. But this is exactly the motivation for LTS methods, because then parallel computing is much more efficient.

4.6.1 Higher order LTS schemes for the convection-diffusion equation

A similar approach, as for the higher order advection LTS schemes, is used to obtain higher order LTS schemes for the linear convection-diffusion equation. The difference is related to the term in front of the second derivative, which needs to be consistent with the physical viscosity. In this case we write the modified equation as

$$U_t + a_1 U_x = a_2 U_{xx} + \sum_{l=3}^{p+1} a_l \frac{\partial^l U}{\partial x^l} + \mathcal{O}(\Delta x^p), \tag{126}$$

From the modified equation (126) we must have $a_1 = a$, $a_2 = \nu$ and $a_l = 0, l = 3, .., p+1$ to achieve a pth order LTS scheme for the advection-diffusion equation. Observe that one more equation needs to be solved to obtain the pth order LTS scheme, therefore we must use a pth order polynomial in this case.

4.6.2 Consistency

We do a consistency analysis for the LTS $\text{CD}\hat{k} - \phi$ schemes applied to the linear convection-diffusion equation. Our $(2(k + \hat{k}) + 1)$-point stencil schemes are given by

$$U_j^{n+1} = U_j^n - \sum_{i=0}^{k-1+\hat{k}} \left(\mathcal{A}_{j-1/2-i}^{i+} \Delta_{j-1/2-i} + \mathcal{A}_{j+1/2+i}^{i-} \Delta_{j+1/2+i} \right), \tag{127}$$

where

$$\Delta_{j+1/2} = U_{j+1} - U_j \tag{128}$$

We rewrite (127)

$$\frac{U_j^{n+1} - U_j^n}{\Delta t} + \frac{1}{\Delta t} \sum_{i=0}^{k-1+\hat{k}} \left(\mathcal{A}_{j-1/2-i}^{i+} \Delta_{j-1/2-i} + \mathcal{A}_{j+1/2+i}^{i-} \Delta_{j+1/2+i} \right) = 0, \tag{129}$$

and define the discrete operator $T_{\Delta t, \Delta x}$ acting on the approximation of $u(x_j, t_n)$ to be

$$T_{\Delta t, \Delta x} U = \frac{U_j^{n+1} - U_j^n}{\Delta t} + \frac{1}{\Delta t} \sum_{i=0}^{k-1+\hat{k}} \left(\mathcal{A}_{j-1/2-i}^{i+} \Delta_{j-1/2-i} + \mathcal{A}_{j+1/2+i}^{i-} \Delta_{j+1/2+i} \right). \tag{130}$$

Next we apply the operator $T_{\Delta t, \Delta x}$ to the exact solution $u(x_j, t_n)$

$$T_{\Delta t, \Delta x} u = \frac{u_j^{n+1} - u_j^n}{\Delta t} + \frac{1}{\Delta t} \sum_{i=0}^{k-1+\hat{k}} \left(\mathcal{A}_{j-1/2-i}^{i+} \Delta_{j-1/2-i} + \mathcal{A}_{j+1/2+i}^{i-} \Delta_{j+1/2+i} \right). \tag{131}$$

Further we Taylor expand the following terms u_j^{n+1}, $\Delta_{j-1/2-i}$ and $\Delta_{j+1/2+i}$:

$$u_j^{n+1} = u_j^n + \Delta t u_t + \frac{\Delta t^2}{2} u_{tt} + \mathcal{O}(\Delta t^3) \tag{132}$$

$$\Delta_{j-1/2-i} = \Delta x u_x - \frac{\Delta x^2}{2}(2i+1)u_{xx} + \frac{\Delta x^3}{3!}(3i^2 + 3i + 1)U_{xxx} + \mathcal{O}(\Delta x^4) \tag{133}$$

$$\Delta_{j+1/2+i} = \Delta x u_x + \frac{\Delta x^2}{2}(2i+1)u_{xx} + \frac{\Delta x^3}{3!}(3i^2 + 3i + 1)U_{xxx} + \mathcal{O}(\Delta x^4) \tag{134}$$

Inserting the equations (132), (133) and (134) into (131), and using the condition that Δt behaves as Δx^2, we get

$$
\begin{aligned}
T_{\Delta t, \Delta x} u = u_t &+ \frac{\Delta x}{\Delta t} \sum_{i=0}^{k-1+\hat{k}} \left(\mathcal{A}^{i+} + \mathcal{A}^{i-} \right) u_x - \frac{\Delta x^2}{2\Delta t} \sum_{i=0}^{k-1+\hat{k}} (2i+1) \left(\mathcal{A}^{i+} - \mathcal{A}^{i-} \right) u_{xx} \\
&+ \frac{\Delta x^3}{3!\Delta t} \sum_{i=0}^{k-1+\hat{k}} (3i^2 + 3i + 1) \left(\mathcal{A}^{i+} + \mathcal{A}^{i-} \right) u_{xxx} + \mathcal{O}(\Delta x^2)
\end{aligned}
\tag{135}
$$

By construction of the LTS CD$\hat{k}$ schemes we have

$$\sum_{i=0}^{k-1+\hat{k}} \left(\mathcal{A}^{i+} + \mathcal{A}^{i-} \right) = C \tag{136}$$

and

$$\sum_{i=0}^{k-1+\hat{k}} (2i+1) \left(\mathcal{A}^{i+} - \mathcal{A}^{i-} \right) - C^2 = \sigma, \tag{137}$$

then equation (135) becomes

$$
\begin{aligned}
T_{\Delta t, \Delta x} u = &u_t + \frac{\Delta x}{\Delta t} C u_x - \frac{\Delta x^2}{2\Delta t} \sigma u_{xx} \\
&+ \frac{\Delta x^3}{3!\Delta t} \sum_{i=0}^{k-1+\hat{k}} (3i^2 + 3i + 1) \left(\mathcal{A}^{i+} + \mathcal{A}^{i-} \right) u_{xxx} + \mathcal{O}(\Delta x^2)
\end{aligned}
\tag{138}
$$

Now let us look at the difference between the differential operator $T = \frac{\partial}{\partial t} + a \frac{\partial}{\partial x} - \nu \frac{\partial^2}{\partial x^2}$ and the discrete operator $T_{\Delta t, \Delta x}$, acting on the function $u(x, t)$

$$T_{\Delta t, \Delta x} u - T u = \frac{\Delta x^3}{3!\Delta t} \sum_{i=0}^{k-1+\hat{k}} (3i^2 + 3i + 1) \left(\mathcal{A}^{i+} + \mathcal{A}^{i-} \right) u_{xxx} + \mathcal{O}(\Delta x^2) \tag{139}$$

given that $\frac{\Delta x}{\Delta t} C = a$ and $\frac{\Delta x^2}{2\Delta t}\sigma = \nu$. The method is consistent because the discrete operator converges to the differential operator when we refine the grid, $T_{\Delta t,\Delta x} u - Tu \to 0$ when $\Delta x \to 0$. The LTS CD$\hat{k} - \phi$ schemes are only first order accurate due to the truncation error of order $\mathcal{O}(\Delta x)$. For higher order methods we use the procedure described in section 4.6.1. Given a and ν in (123), the second order LTS coefficients are defined by

$$\frac{\Delta x}{\Delta t} \sum_{i=0}^{k-1+\hat{k}} \left(\mathcal{A}^{i+} + \mathcal{A}^{i-}\right) = a, \tag{140}$$

$$\frac{\Delta x^2}{2\Delta t} \left(\sum_{i=0}^{k-1+\hat{k}} (2i+1)\left(\mathcal{A}^{i+} - \mathcal{A}^{i-}\right) - C^2 \right) = \nu \tag{141}$$

and

$$\frac{\Delta x^3}{3!\Delta t} \sum_{i=0}^{k-1+\hat{k}} (3i^2 + 3i + 1)\left(\mathcal{A}^{i+} + \mathcal{A}^{i-}\right) = 0. \tag{142}$$

$\mathcal{A}^{i\pm}$ are given by (94) and (95). In this case the function $a(i, C)$ is a quadratic polynomial and the polynomial coefficients are found by solving the system of equations (140)-(142). The stability condition is

$$\Delta t \leq \frac{\Delta x^2 \left(\hat{k}^2 + \frac{1}{4}\right)}{2\nu}. \tag{143}$$

5 Numerical simulations

Now it is time to test the proposed numerical schemes, and evaluate their robustness and accuracy. We divide this chapter into hyperbolic and parabolic problems, mainly focusing on hyperbolic scalar equations and systems of conservation laws. We will cover the linear advection equation, the inviscid Burgers' equation and the Euler equations in the hyperbolic case, and the linear convection-diffusion equation for the parabolic case.

When we do a convergence study we measure the error in the L_1 norm

$$\epsilon(\Delta x, t_n) = ||u_{\text{numerical}} - u_{\text{exact}}||_1 = \Delta x \sum_i |U_i^n - u(x_i, t_n)|, \tag{144}$$

where ϵ is the error at $t_n = n\Delta t$. We find the order of convergence p with the formula

$$p = \frac{\log(\epsilon(\Delta x_1)/\epsilon(\Delta x_2))}{\log(\Delta x_1/\Delta x_2)}, \tag{145}$$

where Δx_1 and Δx_2 are two different grid spacings.

5.1 Hyperbolic problems

5.1.1 The linear advection equation

A convergence analysis is performed for the first, second and third order accurate families of LTS CD$\hat{k}$ schemes applied to the linear advection equation to confirm the accuracy.

$$\frac{\partial u}{\partial t} + a\frac{\partial u}{\partial x} = 0, \tag{146}$$

with a continuous initial condition

$$u(x, t = 0) = \sin(2\pi x). \tag{147}$$

Periodic boundary conditions are implemented and we run the simulation for one period. Then the exact solution is equal to the initial condition $\sin(2\pi x)$. The rates of convergence are listed in tables 2, 4 and 6. As expected the convergence rates are approaching the order of the schemes when the grid is refined. The errors are listed in tables 3, 5 and 7. We observe that the error decreases when the Courant number increases for all the LTS schemes in this analysis. This makes sense, because we are performing fewer iterations. The errors increase when $\hat{k}$ increases. This is probably due to a less accurate approximation of the Riemann problem.

Table 2: Order of convergence p for the first order LTS CD$\hat{k}$ scheme applied to the linear advection equation with a continuous initial condition and $a = 1$.

$\Delta x_1/\Delta x_2$	$C = 1.1$			$C = 2.25$			$C = 4.75$		
	$\hat{k} = 1$	$\hat{k} = 2$	$\hat{k} = 3$	$\hat{k} = 1$	$\hat{k} = 2$	$\hat{k} = 3$	$\hat{k} = 1$	$\hat{k} = 2$	$\hat{k} = 3$
2.00e-02/1.00e-02	0.95	0.83	0.65	1.00	0.93	0.83	0.99	0.96	0.91
1.00e-02/5.00e-03	0.97	0.91	0.81	1.00	0.97	0.92	1.03	1.01	0.98
5.00e-03/2.50e-03	0.98	0.95	0.90	0.99	0.98	0.95	1.01	1.01	0.99
2.50e-03/1.25e-03	0.99	0.98	0.95	1.00	0.99	0.98	1.01	1.00	1.00

Table 3: Error ϵ for the first order LTS CD$\hat{k}$ scheme applied to the linear advection equation with a continuous initial condition and $a = 1$.

Δx	$C = 1.1$			$C = 2.25$			$C = 4.75$		
	$\hat{k} = 1$	$\hat{k} = 2$	$\hat{k} = 3$	$\hat{k} = 1$	$\hat{k} = 2$	$\hat{k} = 3$	$\hat{k} = 1$	$\hat{k} = 2$	$\hat{k} = 3$
2.00e-02	1.1e-1	2.7e-1	4.4e-1	5.5e-2	1.5e-1	2.8e-1	2.7e-2	7.8e-2	1.5e-1
1.00e-02	5.5e-2	1.5e-1	2.8e-1	2.8e-2	8.0e-2	1.6e-1	1.4e-2	4.0e-2	8.2e-2
5.00e-03	2.8e-2	8.0e-2	1.6e-1	1.4e-2	4.1e-2	8.3e-2	6.7e-3	2.0e-2	4.1e-2
2.50e-03	1.4e-2	4.2e-2	8.4e-2	7.0e-3	2.1e-2	4.3e-2	3.3e-3	1.0e-2	2.1e-2
1.25e-03	7.1e-3	2.1e-2	4.4e-2	3.5e-3	1.0e-2	2.1e-2	1.7e-3	5.0e-3	1.0e-2

Table 4: Order of convergence p for the second order LTS CD$\hat{k}$ scheme applied to the linear advection equation with a continuous initial condition and $a = 1$.

$\Delta x_1/\Delta x_2$	$C = 1.1$			$C = 2.25$			$C = 4.75$		
	$\hat{k} = 1$	$\hat{k} = 2$	$\hat{k} = 3$	$\hat{k} = 1$	$\hat{k} = 2$	$\hat{k} = 3$	$\hat{k} = 1$	$\hat{k} = 2$	$\hat{k} = 3$
2.00e-02/1.00e-02	2.00	2.38	2.95	2.00	2.40	2.95	2.00	2.41	2.93
1.00e-02/5.00e-03	2.00	2.13	2.78	2.00	2.14	2.75	1.93	2.09	2.76
5.00e-03/2.50e-03	1.99	2.03	2.49	2.00	2.04	2.43	2.00	2.04	2.44
2.50e-03/1.25e-03	1.99	2.00	2.19	1.98	1.99	2.15	2.00	2.01	2.16

Table 5: Error ϵ for the second order LTS CD$\hat{k}$ scheme applied to the linear advection equation with a continuous initial condition and $a = 1$.

Δx	$C = 1.1$			$C = 2.25$			$C = 4.75$		
	$\hat{k} = 1$	$\hat{k} = 2$	$\hat{k} = 3$	$\hat{k} = 1$	$\hat{k} = 2$	$\hat{k} = 3$	$\hat{k} = 1$	$\hat{k} = 2$	$\hat{k} = 3$
2.00e-02	1.2e-3	1.4e-3	5.1e-3	6.9e-4	8.7e-4	2.9e-3	3.1e-4	4.1e-4	1.4e-3
1.00e-02	3.0e-4	2.7e-4	6.6e-4	1.7e-4	1.6e-4	3.7e-4	7.9e-5	7.6e-5	1.8e-4
5.00e-03	7.6e-5	6.0e-5	9.5e-5	4.3e-5	3.8e-5	5.5e-5	2.1e-5	1.8e-5	2.7e-5
2.50e-03	1.9e-5	1.5e-5	1.7e-5	1.1e-5	9.2e-6	1.0e-5	5.2e-6	4.4e-6	4.9e-6
1.25e-03	4.8e-6	3.7e-6	3.7e-6	2.7e-6	2.3e-6	2.3e-6	1.3e-6	1.1e-6	1.1e-6

Table 6: Order of convergence p for the third order LTS CD$\hat{k}$ scheme applied to the linear advection equation with a continuous initial condition and $a = 1$.

$\Delta x_1/\Delta x_2$	$C = 1.1$			$C = 2.25$			$C = 4.75$		
	$\hat{k} = 2$	$\hat{k} = 3$	$\hat{k} = 4$	$\hat{k} = 2$	$\hat{k} = 3$	$\hat{k} = 4$	$\hat{k} = 2$	$\hat{k} = 3$	$\hat{k} = 4$
2.00e-02/1.00e-02	3.01	3.01	2.99	3.05	3.03	3.02	3.01	3.00	2.99
1.00e-02/5.00e-03	2.99	3.00	2.99	3.01	3.01	3.01	3.03	3.03	3.03
5.00e-03/2.50e-03	3.00	3.00	3.00	2.99	3.00	3.00	3.03	3.02	3.02
2.50e-03/1.25e-03	3.00	3.00	3.00	3.00	3.00	3.00	3.00	3.01	3.01

Table 7: Error ϵ for the third order LTS CD$\hat{k}$ scheme applied to the linear advection equation with a continuous initial condition and $a = 1$.

Δx	$C = 1.1$			$C = 2.25$			$C = 4.75$		
	$\hat{k} = 2$	$\hat{k} = 3$	$\hat{k} = 4$	$\hat{k} = 2$	$\hat{k} = 3$	$\hat{k} = 4$	$\hat{k} = 2$	$\hat{k} = 3$	$\hat{k} = 4$
2.00e-02	1.0e-3	5.0e-3	1.5e-2	6.5e-4	2.8e-3	8.3e-3	3.1e-4	1.3e-3	4.0e-3
1.00e-02	1.3e-4	6.2e-4	1.9e-3	7.9e-5	3.4e-4	1.0e-3	3.9e-5	1.7e-4	5.0e-4
5.00e-03	1.6e-5	7.7e-5	2.4e-4	9.8e-6	4.3e-5	1.3e-4	4.6e-6	2.1e-5	6.1e-5
2.50e-03	2.0e-6	9.7e-6	3.0e-5	1.2e-6	5.3e-6	1.6e-5	5.8e-7	2.5e-6	7.6e-6
1.25e-03	2.5e-7	1.2e-6	3.8e-6	1.5e-7	6.7e-7	2.0e-6	7.3e-8	3.2e-7	9.4e-7

5.1.2 The inviscid Burgers' equation

To see how the LTS CD$\hat{k}$ schemes behave compared to the LTS Roe, the LTS Lax-Friedrichs and the LTS β schemes, we do some numerical simulations on nonlinear PDEs. First we consider a nonlinear scalar equation, then in the next section we move on to a system of nonlinear conservation laws. Here we want to solve the one-dimensional inviscid Burgers' equation

$$\frac{\partial u}{\partial t} + \frac{1}{2}\frac{\partial u^2}{\partial x} = 0, \tag{148}$$

with a square pulse as initial condition

$$u(x, t = 0) = \begin{cases} 1 & 0.3 < x < 0.6 \\ 0 & \text{else} \end{cases} \tag{149}$$

and periodic boundary conditions. We look at the solution after $t = 2s$ and use a grid spacing $\Delta x = 0.01$. The simulation is computed with a Courant number $C = 5$, a relatively high Courant number, see figure 14. The LTS CD1 scheme clearly gives better results in this case than the other schemes. There is no sign of entropy violation from the rarefaction wave and the result is nice and smooth.

For now we have only tried the LTS CD1 scheme. The next step is to compare the LTS CD$\hat{k}$ schemes against each other. Our next simulation has the same conditions as

the one before, but now we compare $\hat{k} = 1$, $\hat{k} = 2$, $\hat{k} = 3$ and $\hat{k} = 4$. As expected the solution is more smeared when we increase $\hat{k}$, see figure 15.
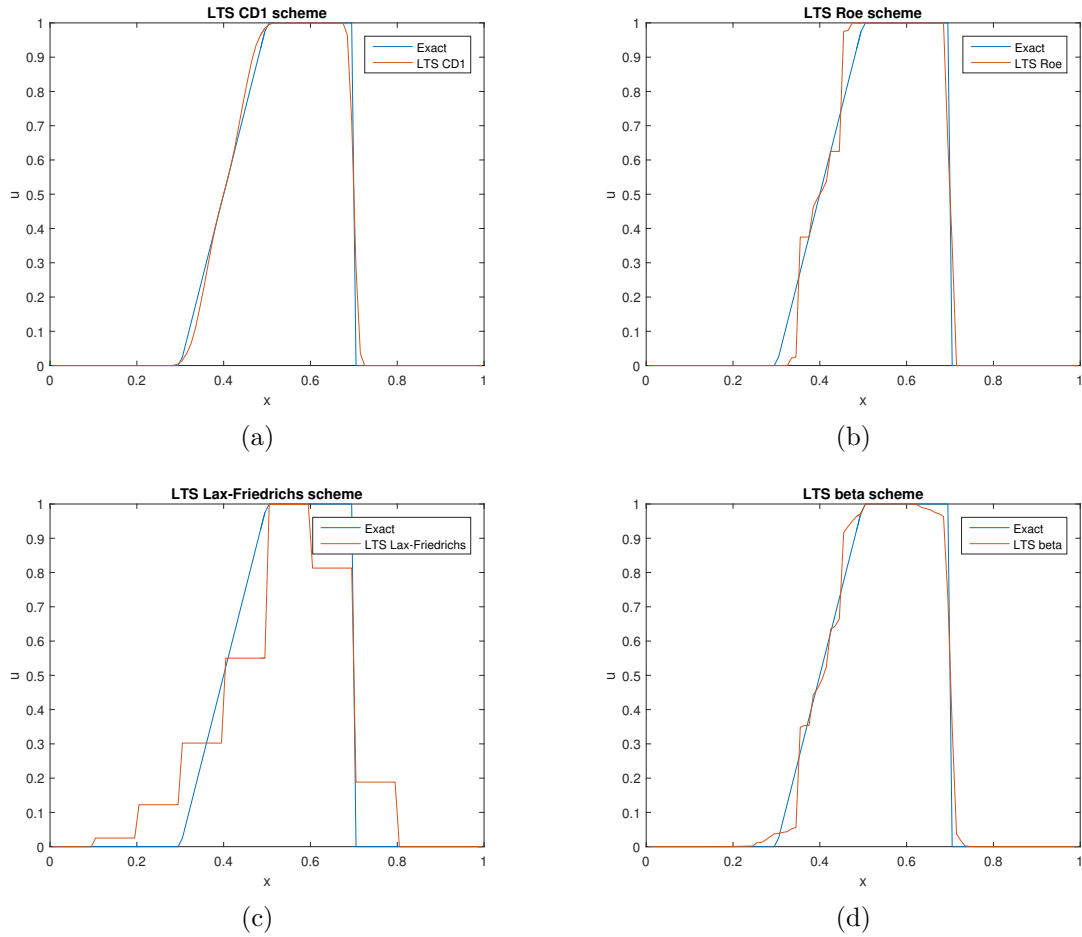

Figure 14: The 1 dimensional inviscid Burgers' equation acting on a square initial pulse, solved with various LTS schemes with 100 cells after $t = 0.2s$. For the LTS β scheme, $\beta = 0.05$. All cases are computed with a Courant number $C = 5$.
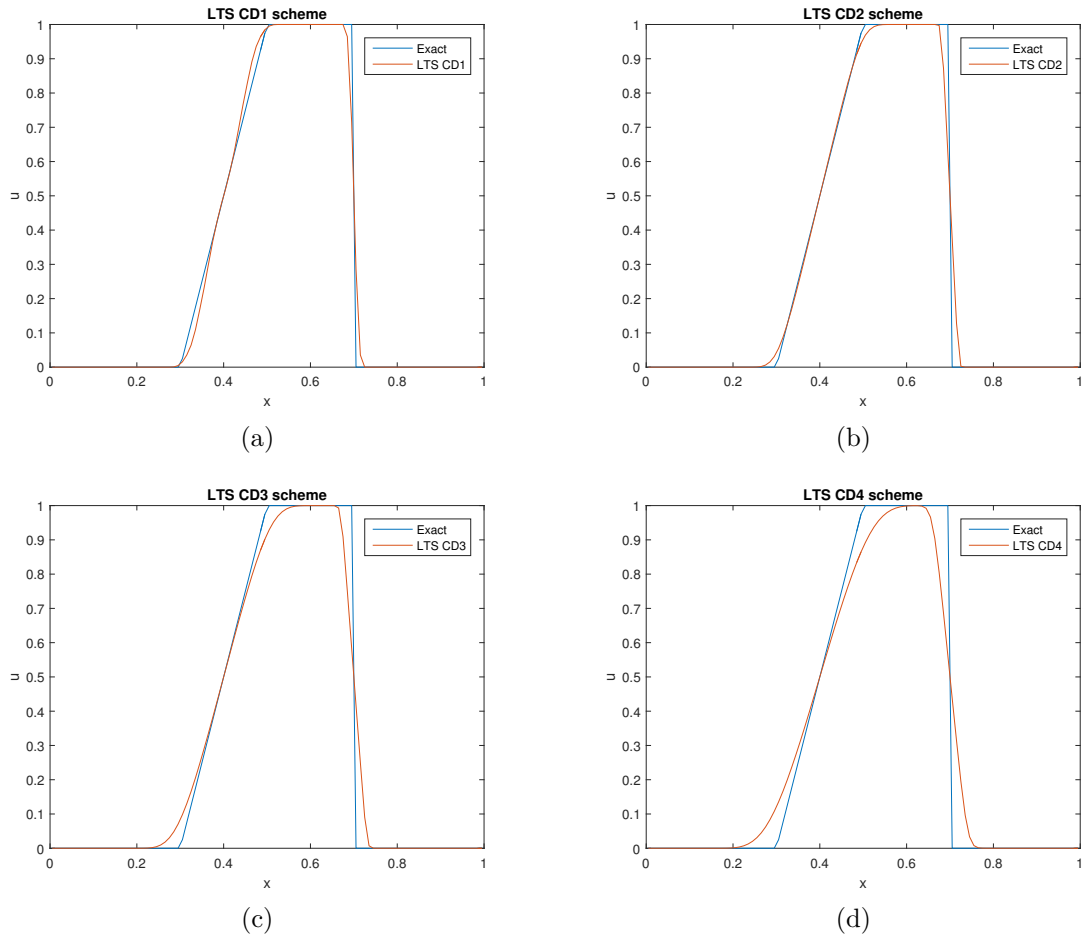
Figure 15: The 1 dimensional inviscid Burgers' equation acting on a square initial pulse, solved with LTS CD$\hat{k}$ ($\hat{k} \in 1, 2, 3, 4$) schemes with 100 cells after $t = 0.2s$. All schemes are computed with a Courant number $C = 5$.

5.1.3 The Euler equations

For the nonlinear system of hyperbolic conservation laws we consider the Euler equations for 1-dimensional gas flow

$$\frac{\partial u}{\partial t} + \frac{\partial f(u)}{\partial x} = 0, \tag{150}$$

with

$$u = \begin{pmatrix} \rho \\ \rho v \\ E \end{pmatrix}, \quad f(u) = \begin{pmatrix} \rho v \\ \rho v^2 + p \\ v(E+p) \end{pmatrix} \tag{151}$$

Here ρ is density, ρv the momentum density, E the density of total energy and p the pressure. We assume an ideal gas, which yields the relation

$$p = (\gamma - 1)\left(E - \frac{1}{2}\rho v^2 \right), \tag{152}$$

where γ is the ratio of specific heat, equal 1.4 for air. As initial condition for our simulation, we will start with constant values for U separated by a single jump in the centre of our computational domain. Let our left and right starting values be

$$\begin{pmatrix} \rho_L \\ p_L \\ v_L \end{pmatrix} = \begin{pmatrix} 1 \\ 1 \\ 0 \end{pmatrix}, \quad \begin{pmatrix} \rho_R \\ p_R \\ v_R \end{pmatrix} = \begin{pmatrix} 0.125 \\ 0.1 \\ 0 \end{pmatrix}. \tag{153}$$

This is referred to as the Sod shock tube problem [19]. The evolution of the density for this problem consists of a left going rarefaction and right going contact and shock discontinuity. The nonlinear Euler equations are linearized through the Roe matrix [20]. One of the challenges in solving the problem numerically with LTS schemes is avoiding entropy violation in the left going rarefaction wave as is observed in the LTS Roe scheme for high Courant numbers. The LTS β scheme helps to smear the solution. Spurious oscillations around the contact discontinuity and shock are also problems for both the LTS Roe and LTS β schemes for very large Courant numbers. For the Sod shock tube problem we compare the numerical and the exact density solution for the schemes discussed this far. The solution is found after $t = 0.25s$ for a Courant number of 8 and 200 computational grid cells, see figure 16. We estimate the optimal β for this problem to behave as $\beta = \min(1, 30\Delta x/L)$ [1], where L is the length of the domain. The LTS Roe and LTS Lax-Friedrichs schemes give very poor results for such a high Courant number. The other two LTS schemes have different ways of adding numerical diffusion, and they are reflected in the simulation. While the LTS CD3 scheme is very smooth, the LTS β scheme shows some tendency to oscillate.

In the next simulation we double the Courant number to $C = 16$, see figure 17, and observe how this affects the schemes. We have in this simulation changed from the LTS CD3 scheme to the LTS CD6 scheme, since more diffusion is needed because of fewer

time steps. From this picture it is even more clear that the LTS β scheme starts to generate wiggles for very high Courant numbers. The LTS CD6 scheme is able to give a smooth solution for this simulation.

In figure 18 we do a grid refinement for the two schemes; the LTS CD6 and the LTS β schemes. We want to see, if oscillations are created for the LTS CD6 scheme, and if the wiggles of the LTS β scheme disappear. Computational domains of 400, 800 1600 cells are tested.

We continue the analysis on the LTS CD$\hat{k}$ schemes, and run simulations of the Euler equations for several Courant numbers with different amounts of numerical diffusion. See figure 19 for results. We find that too little numerical diffusion creates a spike just before the contact discontinuity, and to much numerical diffusion leads to an inaccurate solution. With a visual inspection of the graphs we estimate the ratio $\frac{k}{\hat{k}} = 3$ to give a good trade-off between accuracy and smooth solution.

Finally we see how far it is reasonable to increase the Courant number. We perform the simulations with the above approximation of the stencil width. The results are visualized in figure 20. First we note that there are no indication of spurious oscillations, despite the extremely high Courant numbers. It looks like the method gives smooth solutions for this problem no matter how high we push the Courant number. The simulations are performed on both coarse and refined grids. The solutions are on the other hand very inaccurate, and give more averaged results. The grid spacing decreases for the highest Courant numbers, because the time step becomes larger than the simulation time.

A new simulation is performed with the second order LTS CD$\hat{k} - \phi - 2$ scheme where the ratio $k/\hat{k} = 1$ for Courant numbers 1,2,3 and 10, see figure 21. A general trend for the scheme, like other second order schemes, is oscillations near discontinuities. But we observe with grid refinement that oscillations around the rarefaction and contact discontinuity are damped, for the shock discontinuity they are not damped.

To check the robustness of the LTS CD$\hat{k}$ schemes, we use a test case provided by LeVeque in his paper [7]. This was a double Riemann problem for which the LTS Godunov scheme created spurious oscillations, and might have been one of the reasons why LeVeque did not continue with the LTS method. The initial condition consists of three states U_L, U_M and U_R divided at the points $x = 0.6$ and $x = 0.65$. The states are given by

$$
\begin{pmatrix} \rho_L \\ p_L \\ v_L \end{pmatrix} = \begin{pmatrix} 0.265574 \\ 0.303130 \\ 0.927453 \end{pmatrix}, \quad \begin{pmatrix} \rho_M \\ p_M \\ v_M \end{pmatrix} = \begin{pmatrix} 0.125 \\ 0.1 \\ 0 \end{pmatrix}, \quad \begin{pmatrix} \rho_R \\ p_R \\ v_R \end{pmatrix} = \begin{pmatrix} 0.516633 \\ 1.27472 \\ -2.66908 \end{pmatrix}.
$$
(154)

We show results in figure 22 and 23. The point with this simulation is to give indications that our scheme gives nonoscillating solutions not sacrificing accuracy, for high Courant numbers. The "exact" solution in this case is computed with the Roe scheme with a Courant number $C = 0.875$ and 10000 cells. It is evident that our LTS CD$\hat{k}$ scheme also in this case smears the solution with no oscillations, but there is a

lack of accuracy. With grid refinement we observe convergence to the "exact" solution.
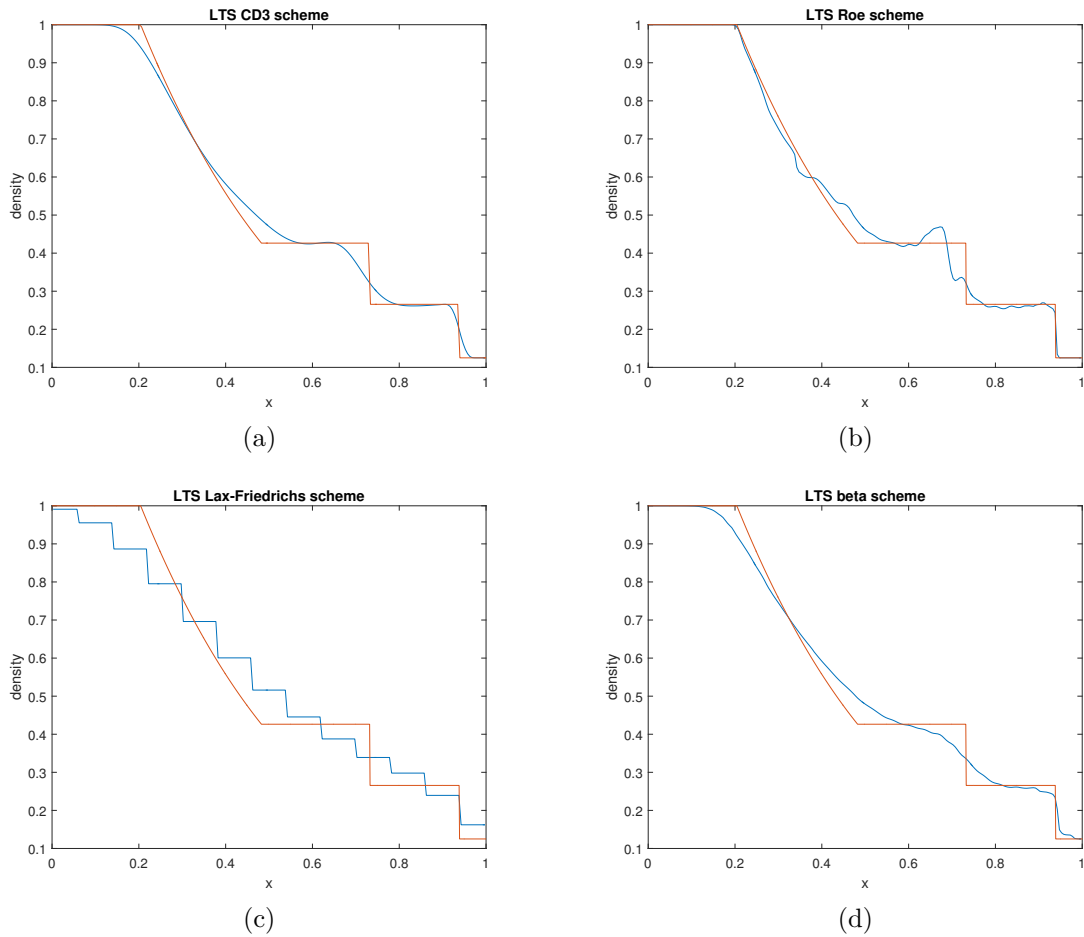
Figure 16: The Sod shock tube problem solved with the LTS CD3, the LTS Roe, the LTS Lax-Friedrichs and the LTS β schemes. The computational domain consists of 200 cells and $\beta = \min(1, 30\Delta x/L)$, and all schemes are computed with a Courant number $C = 8$.
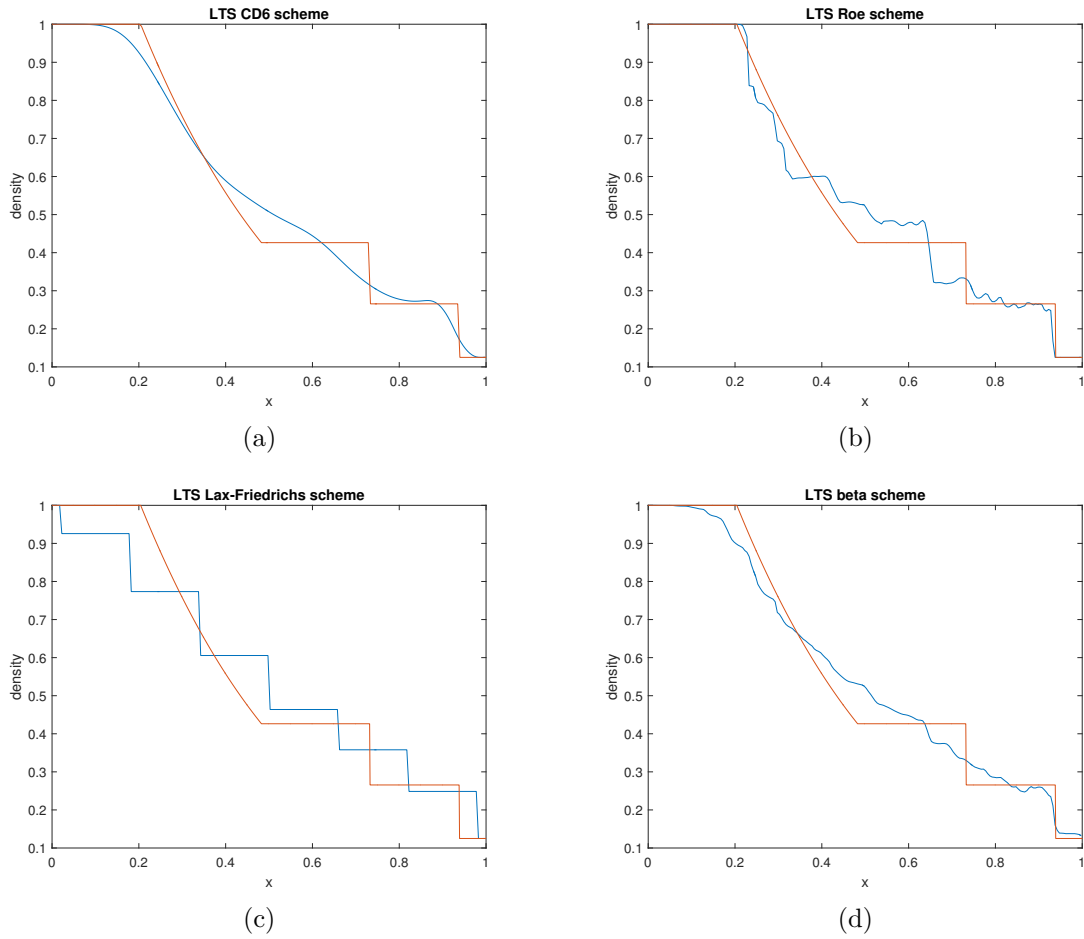
Figure 17: The Sod shock tube problem solved with the LTS CD6, the LTS Roe, the LTS Lax-Friedrichs and the LTS β schemes. The computational domain consists of 200 cells and $\beta = \min(1, 30\Delta x/L)$, and all schemes are computed with a Courant number $C = 16$.
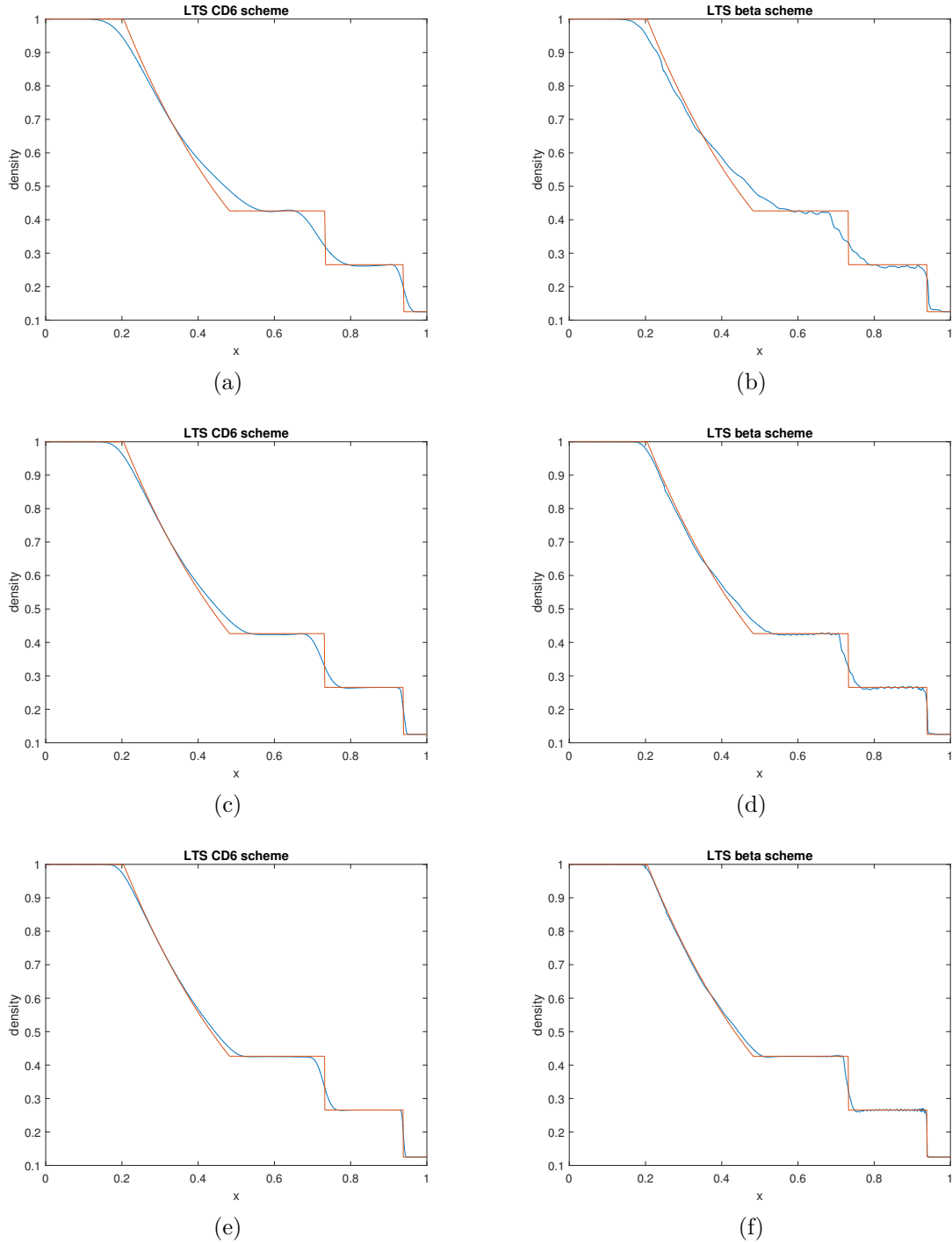
Figure 18: The Sod shock tube problem solved with the LTS CD6 and the LTS β schemes. The computational domain consists of 400, 800 and 1600 cells ranked from top to bottom. $\beta = \min(1, 30\Delta x/L)$, and all simulations are computed with a Courant number $C = 16$.
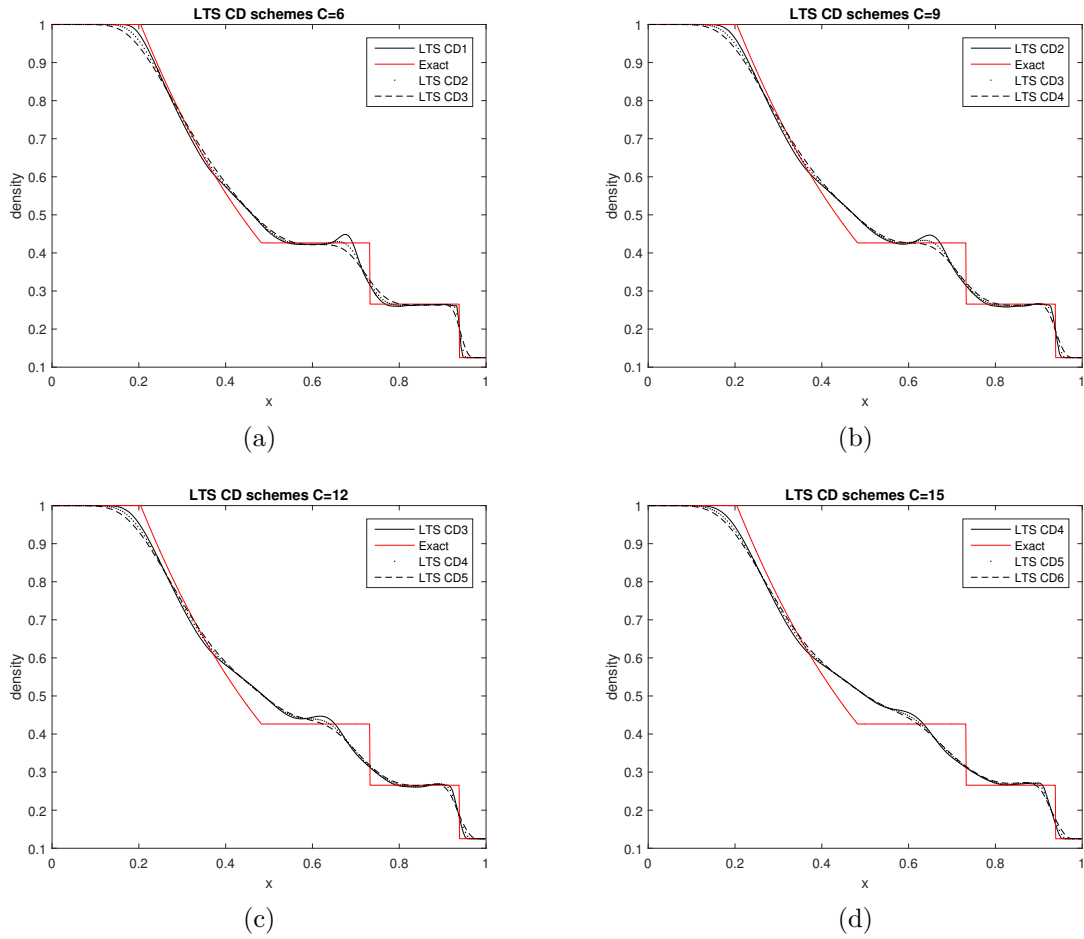
Figure 19: The Sod shock tube problem solved for Courant numbers 6, 9, 12 and 15 with different amounts of added numerical diffusion. The computational domain consists of 200 cells.
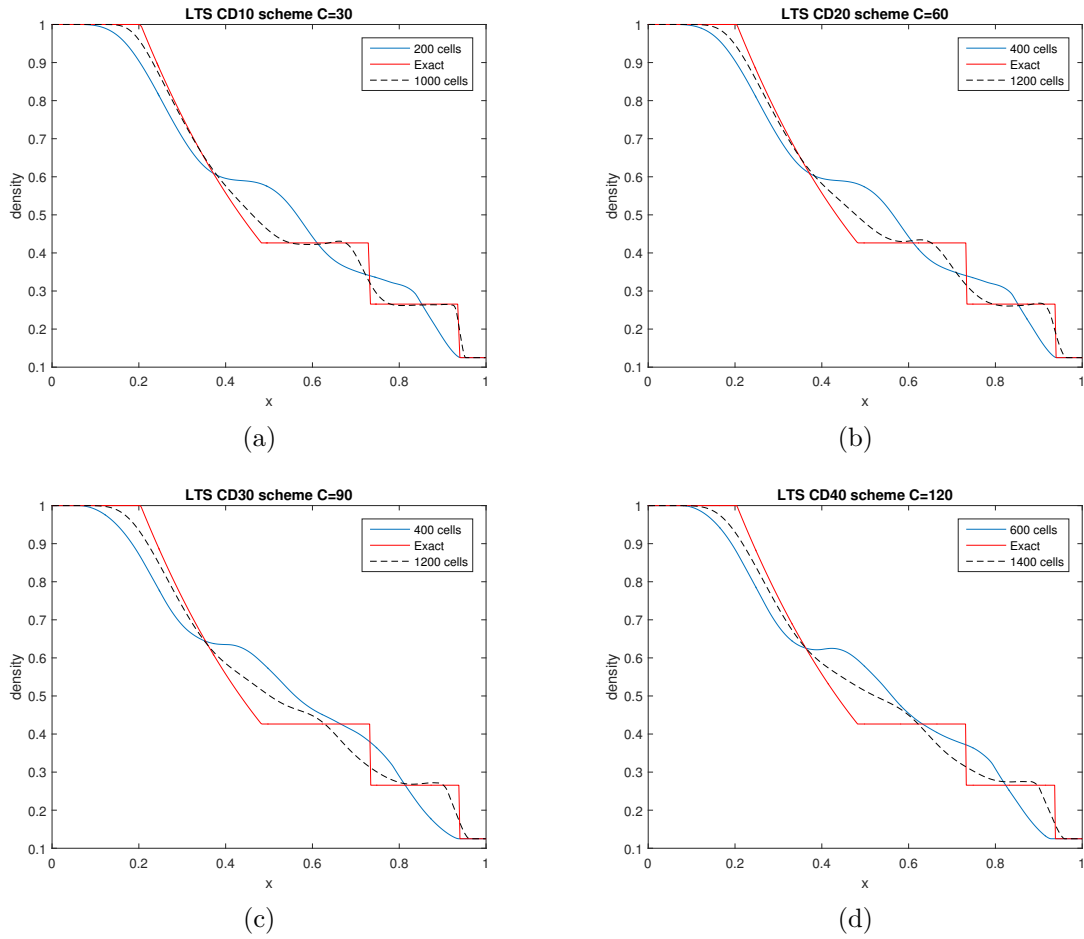
Figure 20: The Sod shock tube problem solved for Courant numbers 30, 60, 90 and 120 with a LTS CD$\hat{k}$ scheme corresponding to the ratio $\frac{k}{\hat{k}} = 3$. The computational domains consist of both a course grid and a fine grid.
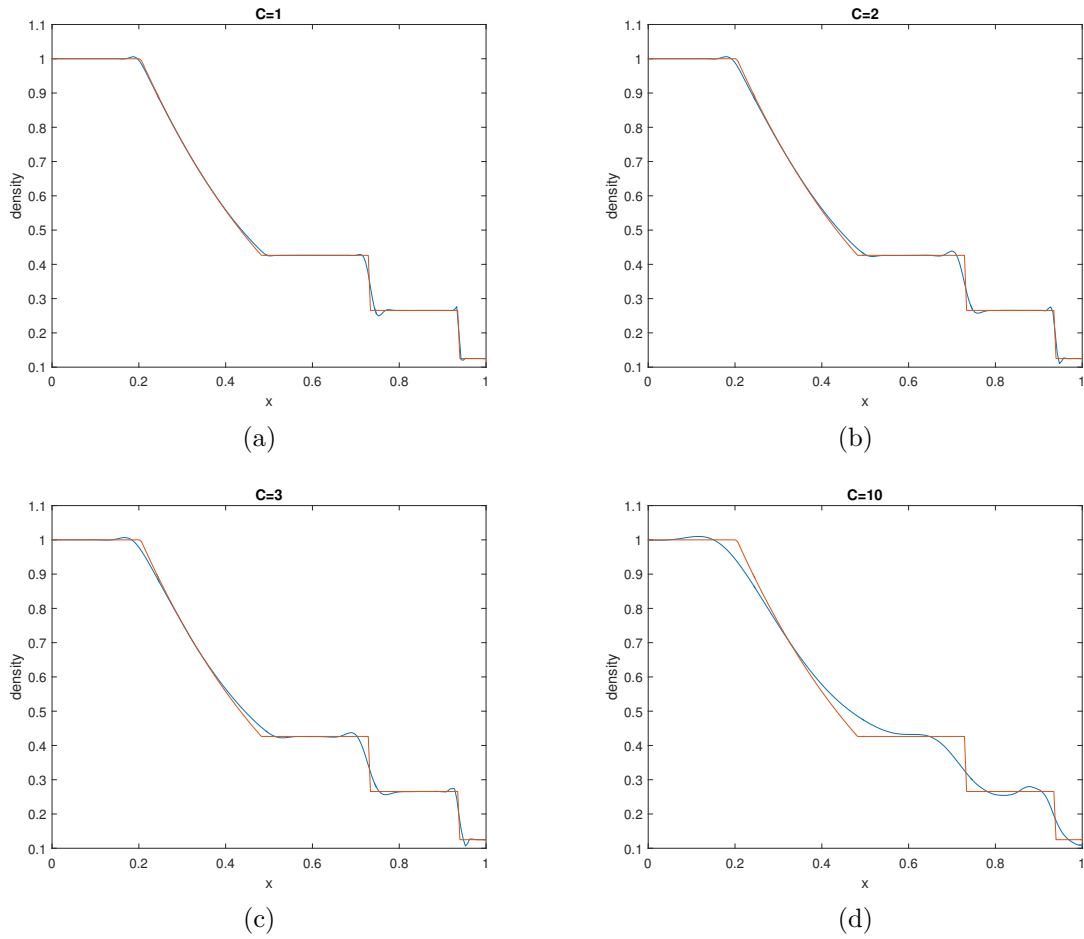
Figure 21: The Sod shock tube problem solved for Courant numbers 1, 2, 3 and 10 with the second order LTS CD$\hat{k} - \phi - 2$ scheme corresponding to the ratio $\frac{k}{\hat{k}} = 1$. The computational domain consists of 200 cells.
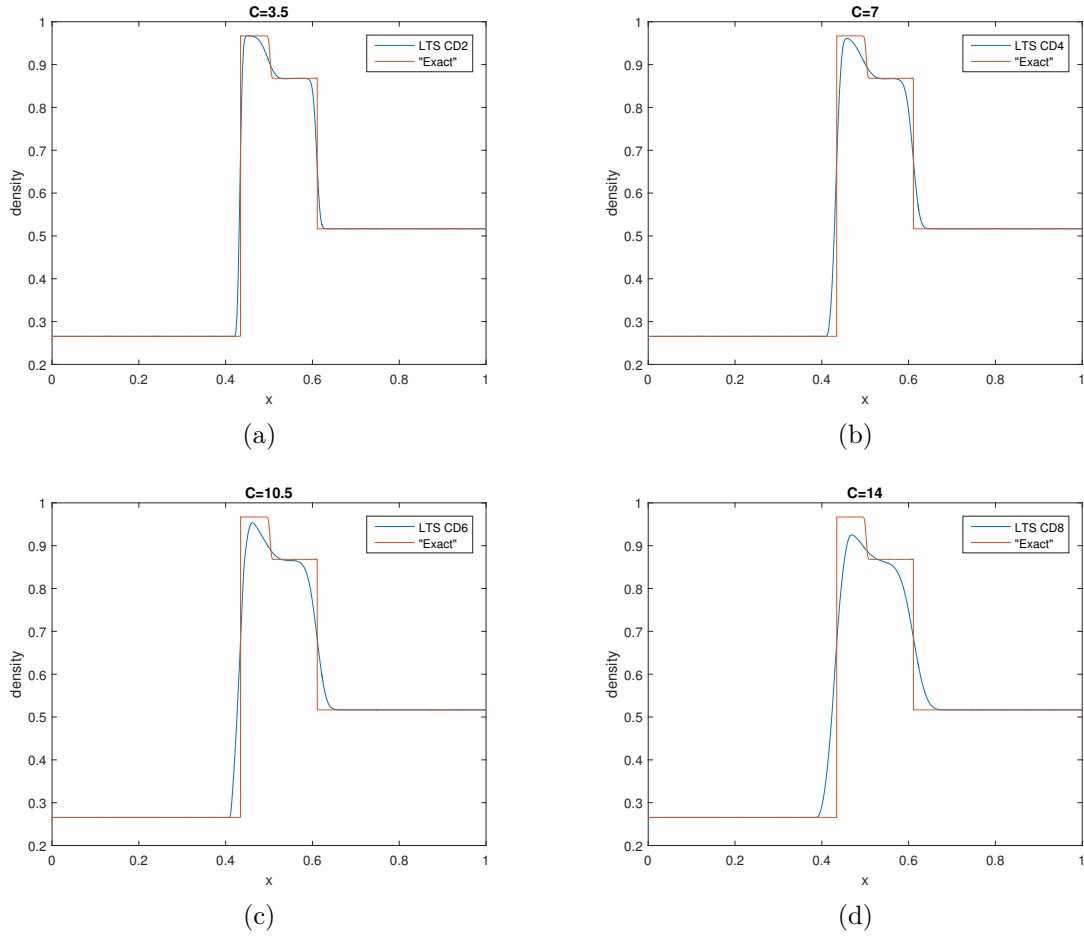
Figure 22: LeVeques test case solved for Courant numbers 3.5, 7, 10.5 and 14 with 400 cells and an appropriate LTS CD$\hat{k}$ scheme where $\hat{k} = 2, 4, 6, 8$, respectively.
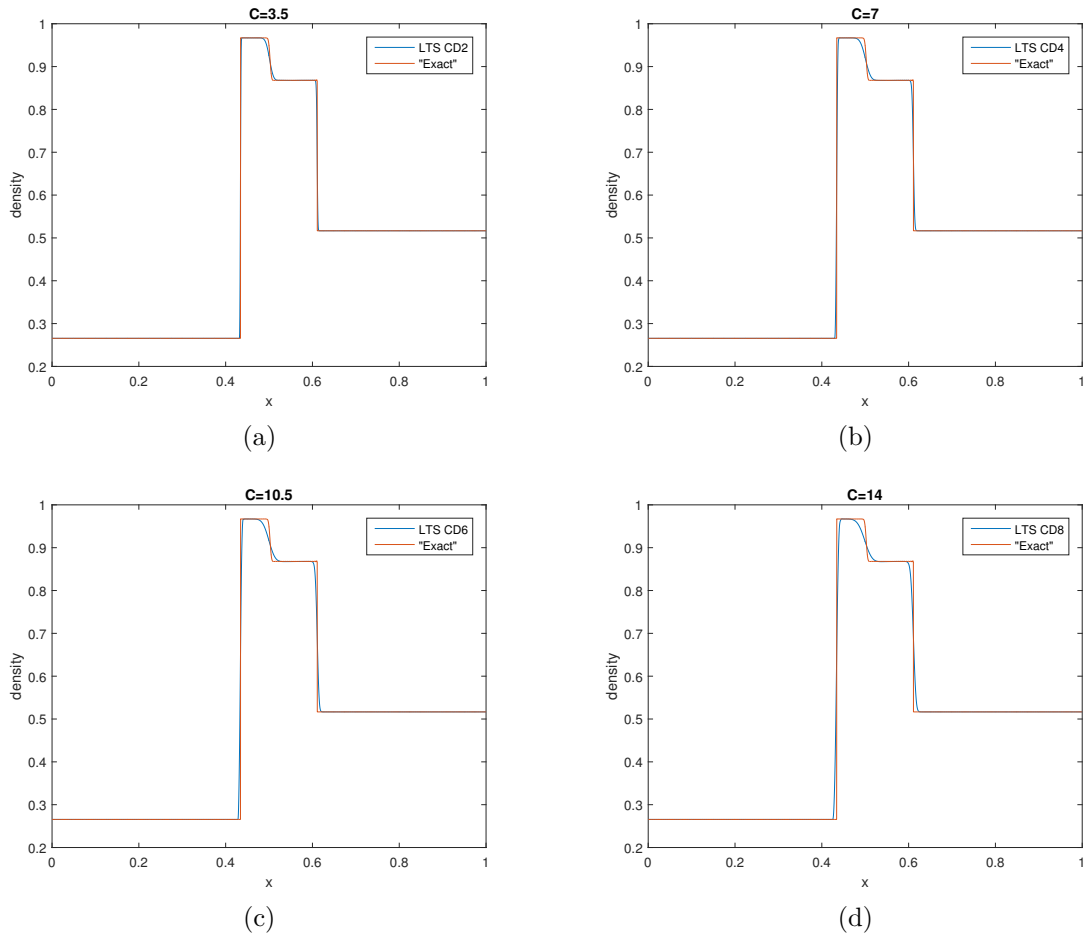
Figure 23: LeVeques test case solved for Courant numbers 3.5, 7, 10.5 and 14 with 2000 cells and an appropriate LTS CD$\hat{k}$ scheme where $\hat{k} = 2, 4, 6, 8$, respectively.

5.2 Parabolic problem

5.2.1 The convection-diffusion equation

Simulations are performed on a Gauss function as initial condition, which is the fundamental solution of the diffusion equation

$$\frac{\partial u}{\partial t} = \nu \frac{\partial^2 u}{\partial x^2}, \tag{155}$$

given by

$$u(x,t) = \frac{2}{\sqrt{4\pi\nu t}} e^{-\frac{x^2}{4\nu t}} \tag{156}$$

The linear convective term $a\frac{\partial u}{\partial x}$ only contributes by translating the solution in space. Thus the fundamental solution to the linear convection-diffusion equation is

$$u(x,t) = \frac{2}{\sqrt{4\pi\nu t}} e^{-\frac{(x-at)^2}{4\nu t}} \tag{157}$$

In equation (157) we have a singularity for $t = 0$, therefore we let our initial condition for (123) be

$$u(x,t_1) = \frac{2}{\sqrt{4\pi\nu t_1}} e^{-\frac{x^2}{4\nu t_1}}, \tag{158}$$

starting at time $t = t_1$, with an exact solution after t_{max}

$$u(x,t_{max}) = \frac{2}{\sqrt{4\pi\nu(t_1 + t_{max})}} e^{-\frac{(x-at_{max})^2}{4\nu(t_1+t_{max})}}. \tag{159}$$

Table 8: Order of convergence p for a second order LTS CD$\hat{k}$ scheme applied to the linear convection-diffusion equation with a Gauss function as initial condition, for different ratios r and $\hat{k}$. The advection speed is $a = 1$ and the simulation runs for $t_{max} = 0.025$. The length of the domain L is 20.

$\Delta x_1/\Delta x_2$	$\hat{k} = 2$			$\hat{k} = 20$	$\hat{k} = 20$	$\hat{k} = 10$
	$r = 5$	$r = 10$	$r = 20$	$r = 0.1$	$r = 0.5$	$r = 1$
2.00e-02/1.00e-02	2.01	2.11	2.09	2.11	2.43	2.13
1.00e-02/5.00e-03	2.01	2.00	2.03	1.99	1.99	2.07
5.00e-03/2.50e-03	2.00	2.00	2.02	2.01	2.00	2.02

We do a convergence analysis of a second order LTS CD$\hat{k}$ scheme modified for convection-diffusion problems, see section 4.6. Rates of convergence values p are given in table 8 for different ratios $r = a/\nu = Re/L$ and for different $\hat{k}$. Re is the Reynolds number and L is the length of the domain. Notice that a high ratio is evaluated with a small stencil extension ($\hat{k} = 2$) and a low ratio with a larger stencil extension. The reason is that the Riemann problem becomes more smeared with more diffusion. Then a larger $\hat{k}$ gives a better approximation of the Riemann Problem. This is the most efficient way to do it, because the stencil becomes unnecessary wide if large $\hat{k}$ is used for convection dominated flow.

6 Conclusions and further work

We have designed a family of LTS schemes with a robust way of adding numerical viscosity to hyperbolic conservation laws for high Courant numbers. We have introduced a parameter $\hat{k}$ which increases the numerical viscosity. If oscillations occur in the solution, we smear them by increasing $\hat{k}$. Several simulations on the Euler equations with different initial conditions are performed and the scheme gives oscillation-free solutions for appropriate choices of $\hat{k}$. A further study on optimal choices of $\hat{k}$ would be advantageous for practical implementation. Maybe there exists some kind of relationships between $\hat{k}$, the Courant number and physical parameters.

Higher order LTS schemes are constructed and applied to both linear and nonlinear PDEs, with promising results. A second order LTS scheme, used to solve the Sod shock tube problem, has remarkably good accuracy and is a good candidate for further analyses. In particular a problem with oscillations around discontinuities needs to be improved. A first thought is to degrade the scheme to a first order non oscillating scheme in the vicinity of a discontinuity [8, 12].

A von Neumann stability analysis for a local $(2k + 1)$-point scheme is carried out and can be used to verify linear stability for the schemes (61). We have in addition given algebraic proofs that any $(2k+1)$-point TVD scheme is also linearly stable in the sense of von Neumann and further that a $(2k + 1)$-point linearly stable scheme implies positive or zero numerical viscosity.

The LTS method is extended to parabolic PDEs through a natural extension of the LTS CD$\hat{k}$ scheme. First simulations with the constant coefficient time dependent convection-diffusion equation on a Gauss function have been successful. The method applies to all ratios of convection to diffusion, and can be extended to higher order. The constant coefficient case is the simplest case, but the method has potential to work on more complicated problems, like the viscous Burgers' equation with a coordinate dependent diffusion coefficient, i.e. $\nu = \nu(x)$.

References

[1] Lindqvist, S., Aursand, P., Flåtten, T. and Solberg, A. A. (2015). Large time step TVD schemes for hyperbolic conservation laws. Accepted for SIAM Journal on Numerical Analysis.

[2] LeVeque, R. J. (2002). Finite Volume Methods for Hyperbolic Problems. Cambridge Texts in Applied Mathematics. Cambridge University Press.

[3] Colombo, R. M. (2002). A 2x2 Hyperbolic Traffic Flow Model, Mathematical and Computer Modelling 35 683-688.

[4] Courant, R., Friedrichs, K., Lewy, H. (1967), On the partial difference equations of mathematical physics, IBM Journal of Research and Development 11 (2): 215–234.

[5] LeVeque, R. J. (1982). Large time step shock-capturing techniques for scalar conservation laws. SIAM Journal on Numerical Analysis, 19(6):1091–1109.

[6] LeVeque, R. J. (1984). Convergence of a large time step generalization of Godunov's method for conservation laws. Communications on Pure and Applied Mathematics, 37(4):463–477.

[7] LeVeque, R. J. (1985). A large time step generalization of Godunovs method for systems of conservation laws. SIAM Journal on Numerical Analysis, 22(6):1051–1073.

[8] Harten, A (1986), On a large time-step high resolution scheme. Mathematics of Computation, 46(174):379-399.

[9] Qian, Z., Lee, C.-H. (2011). A class of large time step Godunov schemes for hyperbolic conservation laws and applications. Journal of Computational Physics 230, 7418–7440.

[10] Qian, Z., Lee, C.-H. (2012). On large time step TVD scheme for hyperbolic conservation laws and its efficiency evaluation. Journal of Computational Physics 231, 7415–7430.

[11] Morales-Hernández M., Hubbard M.E., García-Navarro P. (2014). A 2D extension of a Large Time Step explicit scheme for unsteady problems with wet/dry boundaries. Journal of Computational Physics 263, 303–327.

[12] Bore, S. L. (2015). High-Resolution Large Time-Step Schemes for Hyperbolic Conservation Laws, master's thesis. NTNU.

[13] Pletcher, R. H., Tannehill, J. C., Anderson, D. A. (2013). Computational Fluid Mechanics and Heat Transfer, 3rd edition, CRC Press, Boca Raton.

[14] Osher, S. (1984). Riemann solvers, the entropy condition, and difference approximations, SIAM J. Numer. Anal. 21, 217–235.

[15] Harten, A (1984), On a class of high resolution total-variation-stable finite-difference schemes. SIAM J. Numer. Anal. Vol. 21, No. 1, 1–23.

[16] Lindqvist, S. (2014). Large time step schemes, summer report. Internal SINTEF memo.

[17] Solberg, A.A. (2015). Large Time Step methods for fluid flow problems. Project work.

[18] Abramowitz, M., Stegun, I. A. (1964). Handbook of Mathematical Functions with Formulas, Graphs, and Mathematical Tables. Applied Mathematics Series 55 Washington D.C., USA; New York, USA: United States Department of Commerce, National Bureau of Standards; Dover Publications.

[19] Sod, G. A. (1978). A Survey of Several Finite Difference Methods for Systems of Nonlinear Hyperbolic Conservation Laws. J. Comput. Phys. 27: 1–31.

[20] Roe, P. L. (1981a). Approximate Riemann solvers, parameter vectors, and difference schemes. Journal of Computational Physics, 43:357-372.